DFT Study on the CuBr-Catalyzed Synthesis of Highly Substituted Furans: Effects of Solvent DMF, Substrate MeOH, Trace H_2O and Metallic Valence State of Cu

Binfang Yuan, Rongxing He, Wei Shen, Weixia Hu, Ming Li*

Key Laboratory of Luminescence and Real-Time Analytical chemistry (Southwest University), Ministry of Education, College of Chemistry and Chemical Engineering, Southwest University, Chongqing 400715, China

* To whom correspondence should be addressed. E-mail: liming@swu.edu.cn

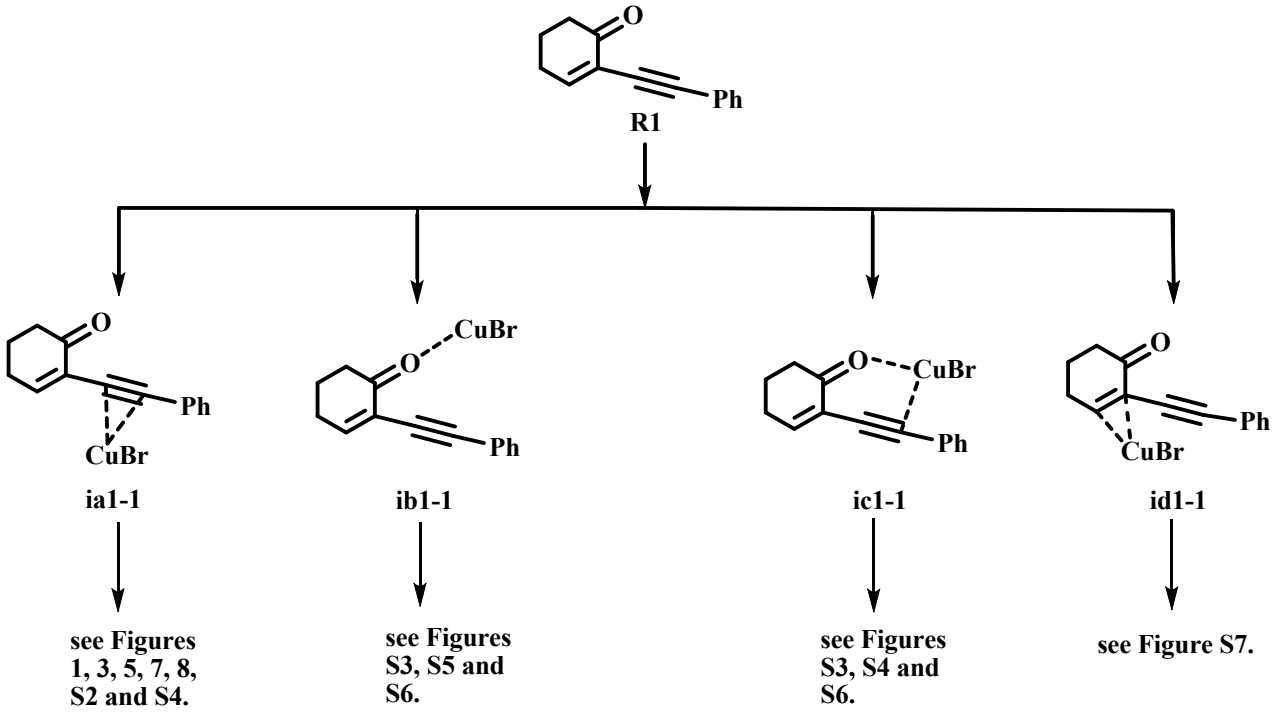

Figure S1. Four coordination models of CuBr with 2-(1-alkynyl)-2-alken-1-ones (R1).

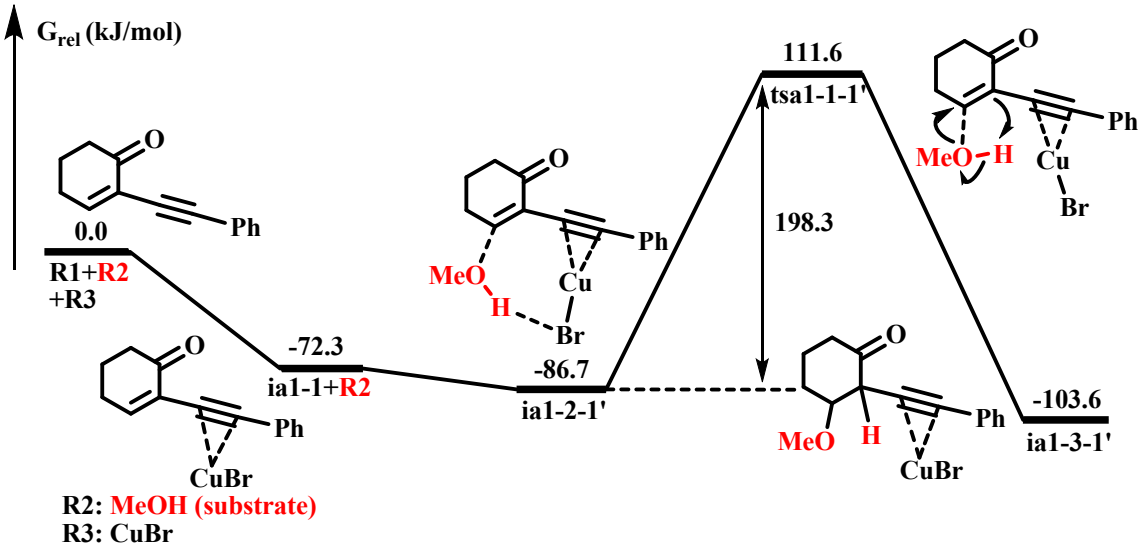

Figure S2. DFT-computed energy profiles for the coordination model CuBr/C1-C2 to synthesize highly substituted furans without the participation of cocatalysts.

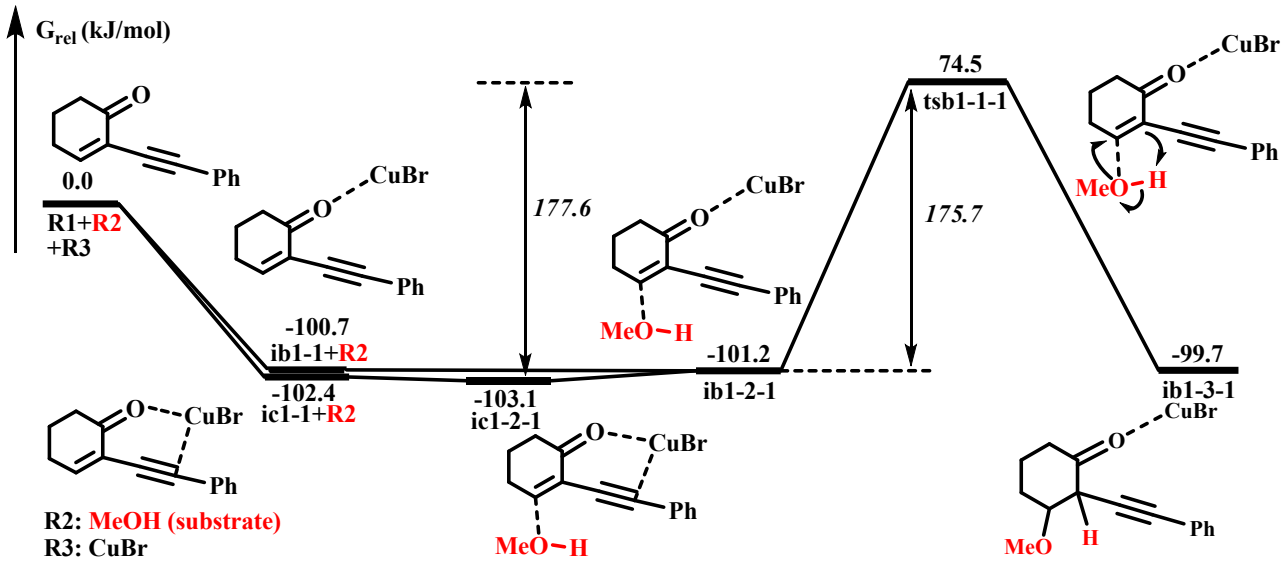

Figure S3. DFT-computed energy profiles for the coordination models CuBr/O1 and CuBr/(C1-C2 and O1) to synthesize highly substituted furans without the participation of cocatalysts.

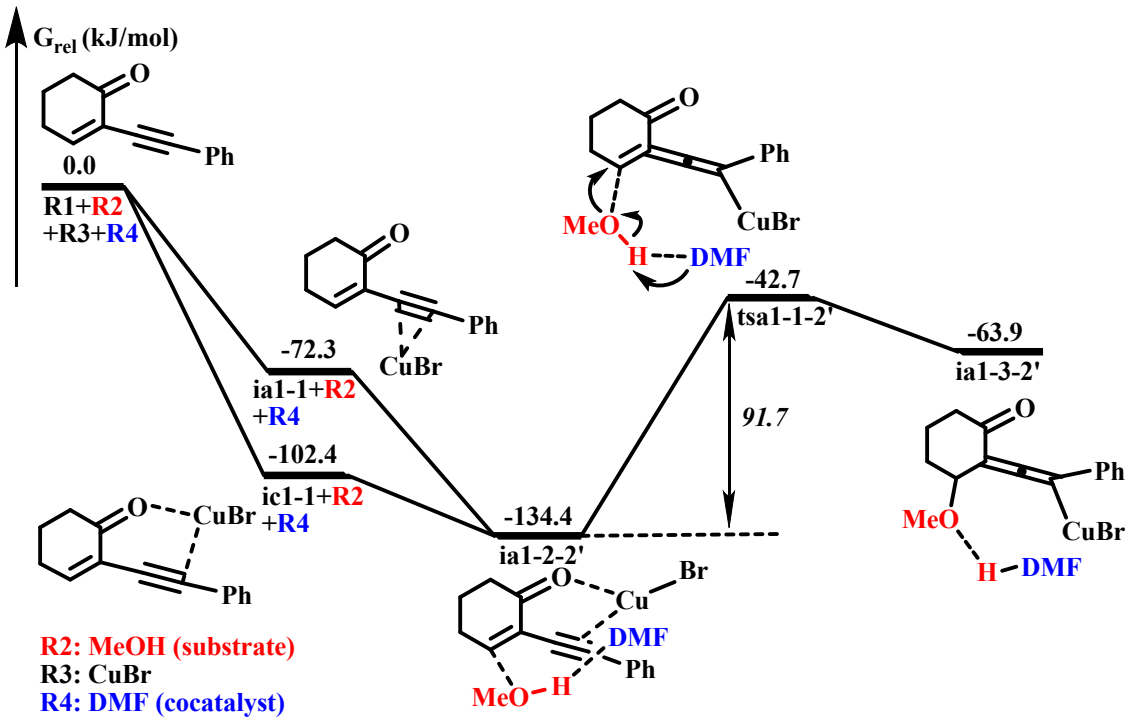

Figure S4. DFT-computed energy profiles for the coordination models CuBr/C1-C2 and CuBr/(C1-C2 and O1) to synthesize highly substituted furans with the participation of DMF.

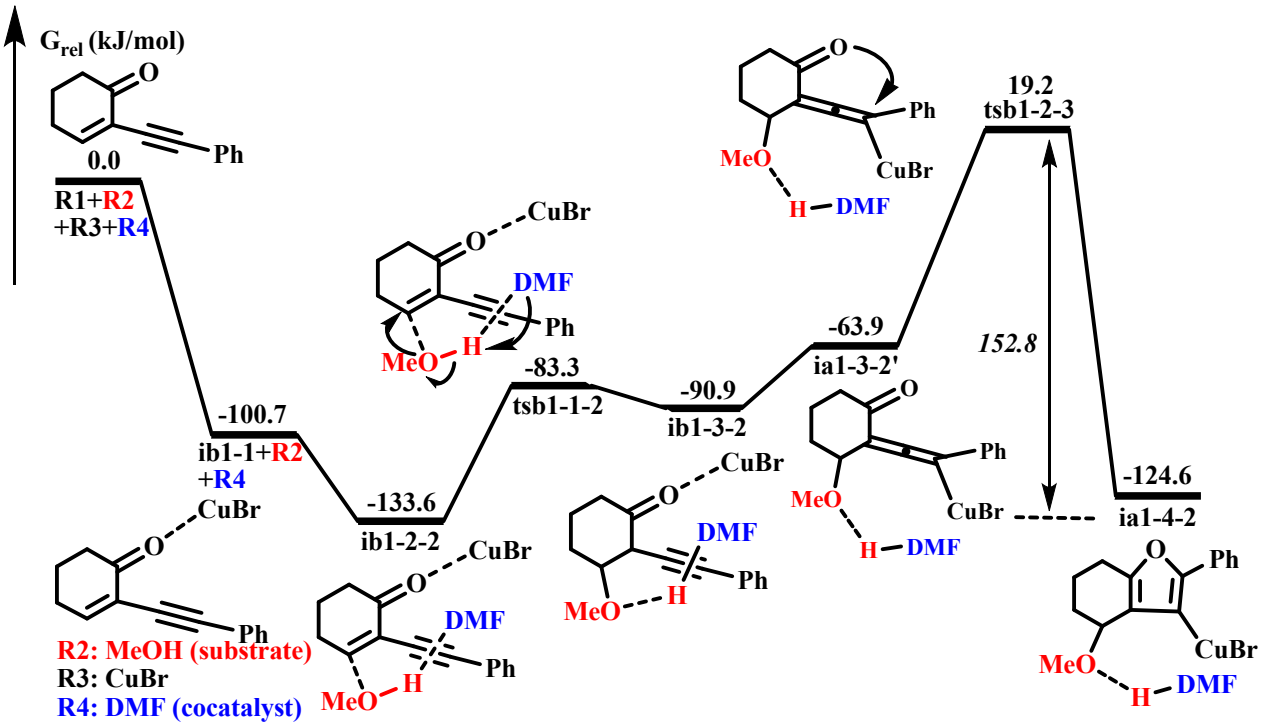

Figure S5. DFT-computed energy profiles for the coordination model CuBr/O1 to synthesize highly substituted furans with the participation of DMF.

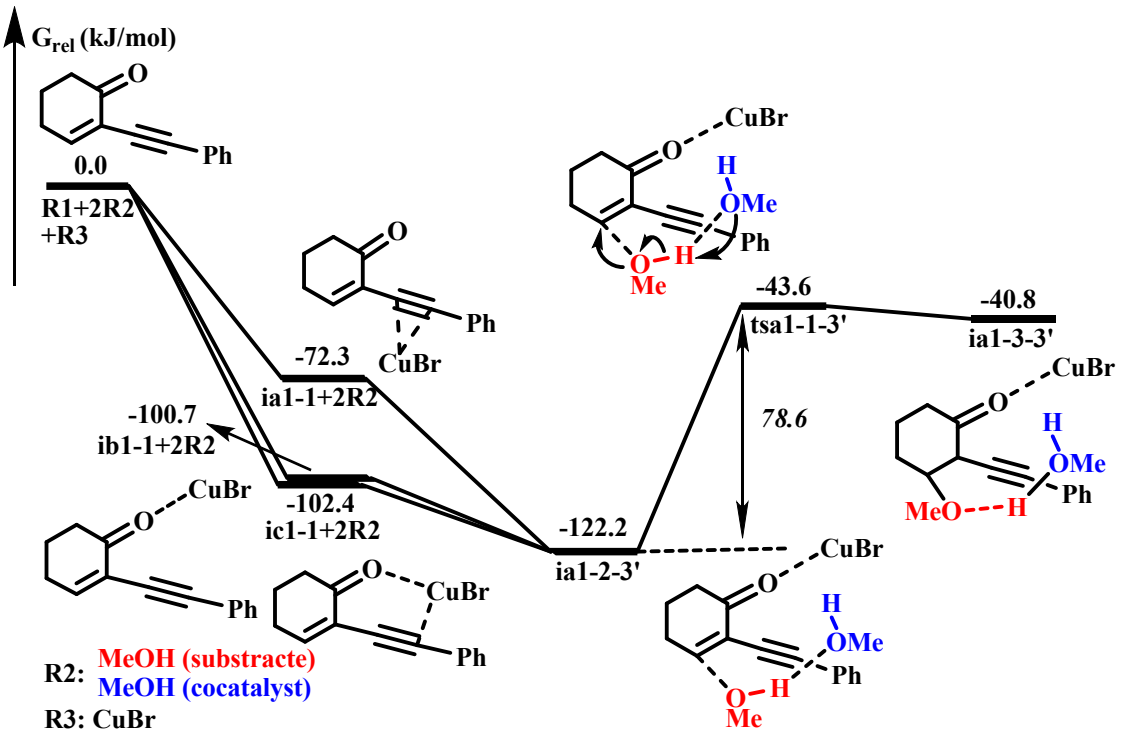

Figure S6. DFT-computed energy profiles for the coordination models CuBr/C1-C2, CuBr/(C1-C2 and O1) and CuBr/O1 to synthesize highly substituted furans with the participation of MeOH.

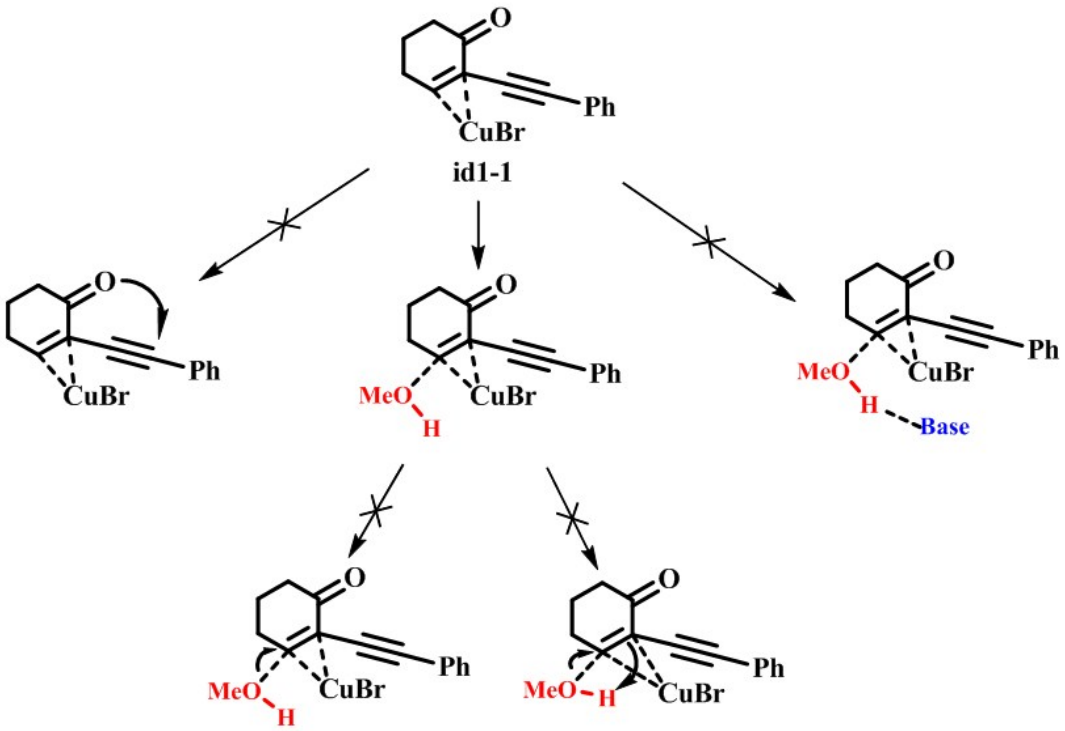

.

Figure S7. The coordination case of CuBr with C3-C4.

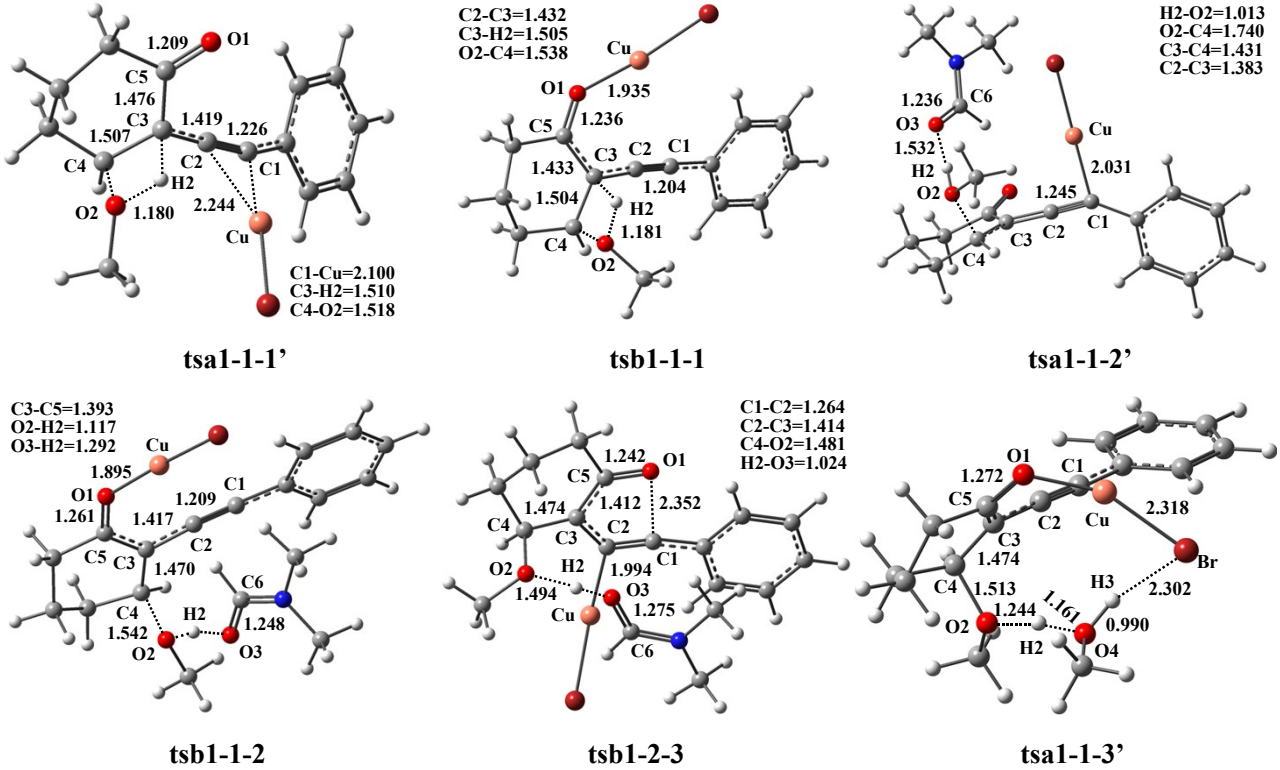

tsa1-1-1' **tsb1-1-1** **tsa1-1-2'**

tsb1-1-2 **tsb1-2-3** **tsa1-1-3'**

Figure S8. The key geometrical structures of Figures S2-S6 (selected structural parameters are listed (bond lengths in Å)).

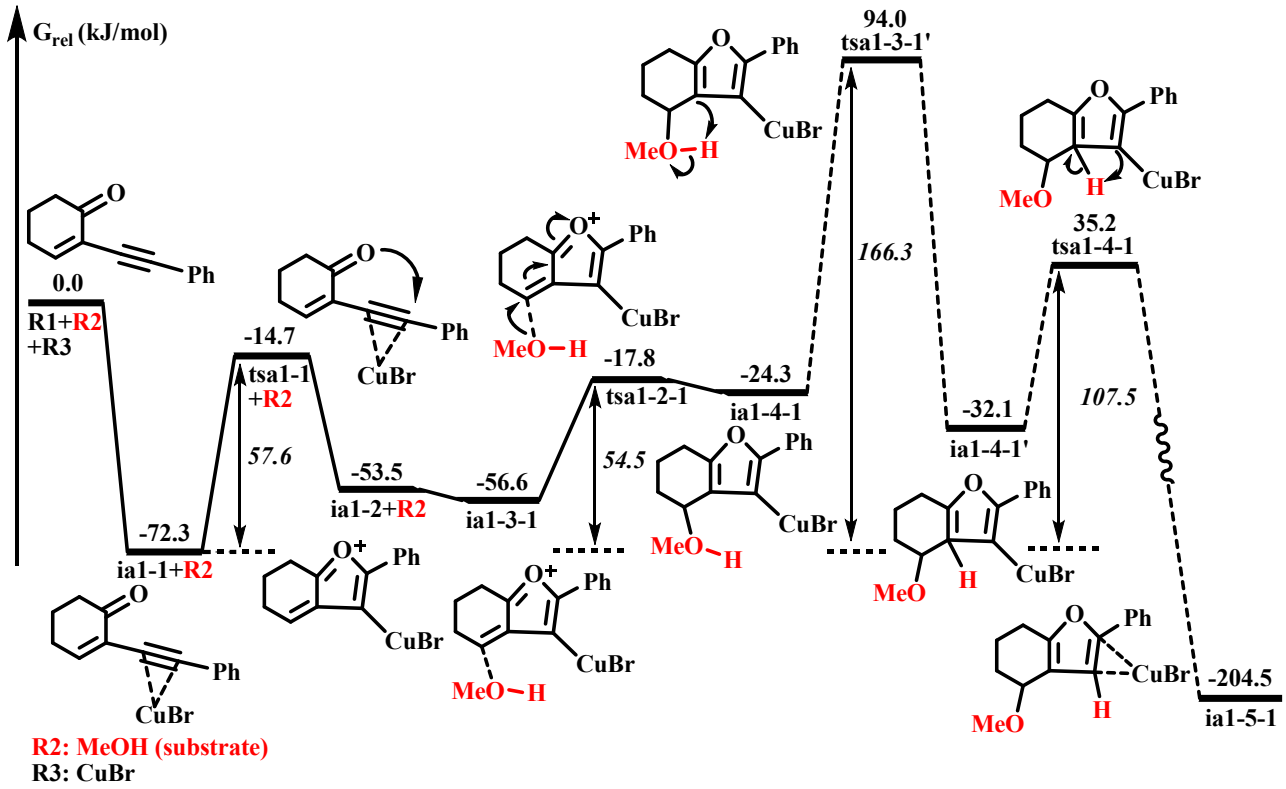

Figure S9. DFT-computed energy profile for the CuBr-catalyzed synthesis of high substituted furans without the participation of cocatalysts.

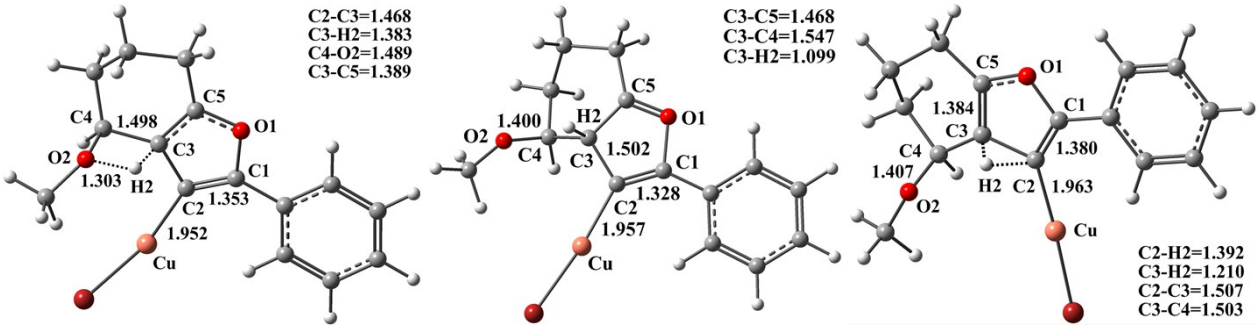

tsa1-3-1' **ia1-4-1'** **tsa1-4-1**

Figure S10. Optimized structures for the two-step H-transfer process in CuBr-catalyzed synthesis of high substituted furans without the participation of cocatalysts (selected structural parameters are listed (bond lengths in Å).

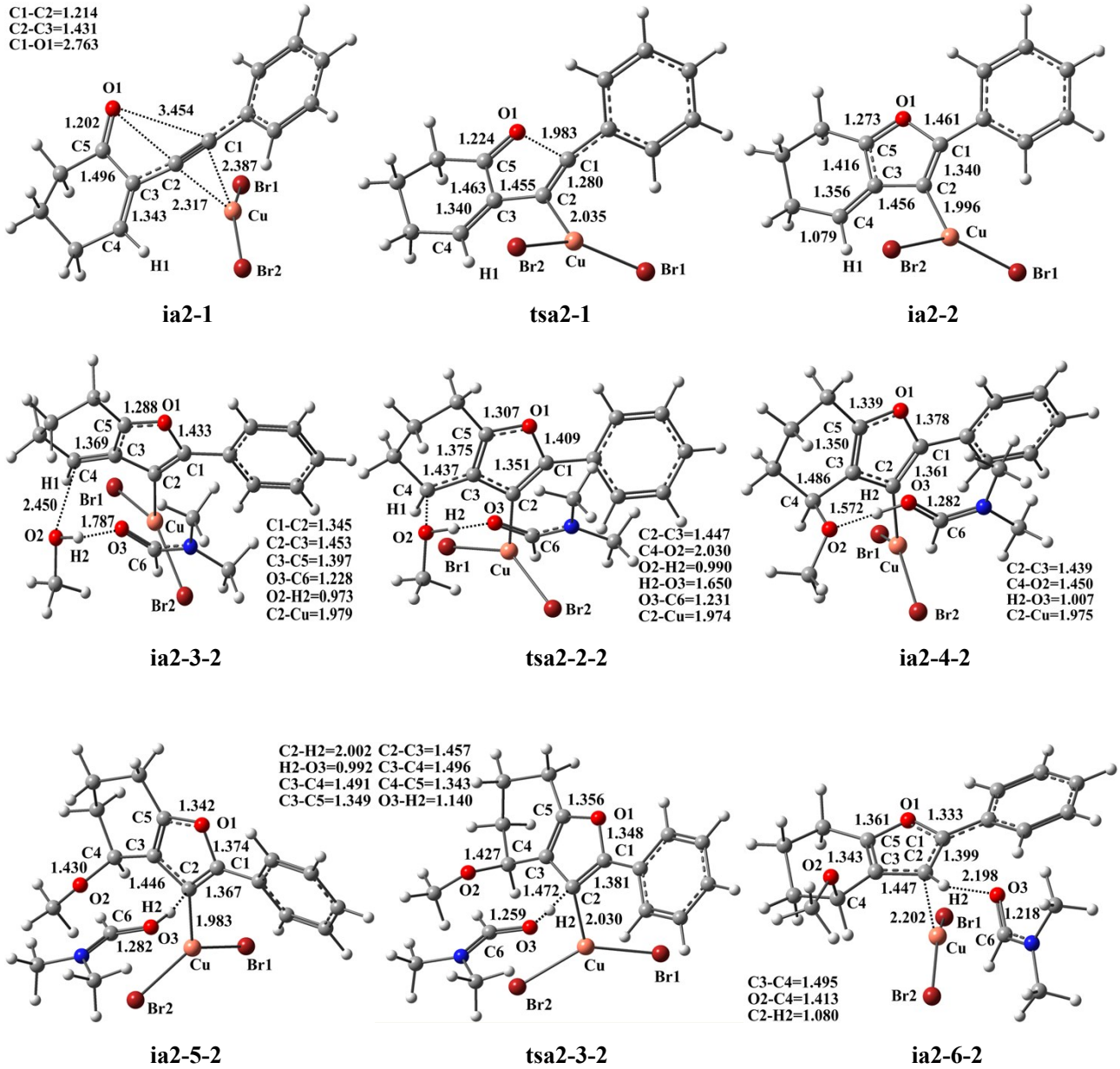

Figure S11. Optimized structures for the $CuBr_2$-catalyzed synthesis of high substituted furans with the participation of DMF (selected structural parameters are listed (bond lengths in Å)).

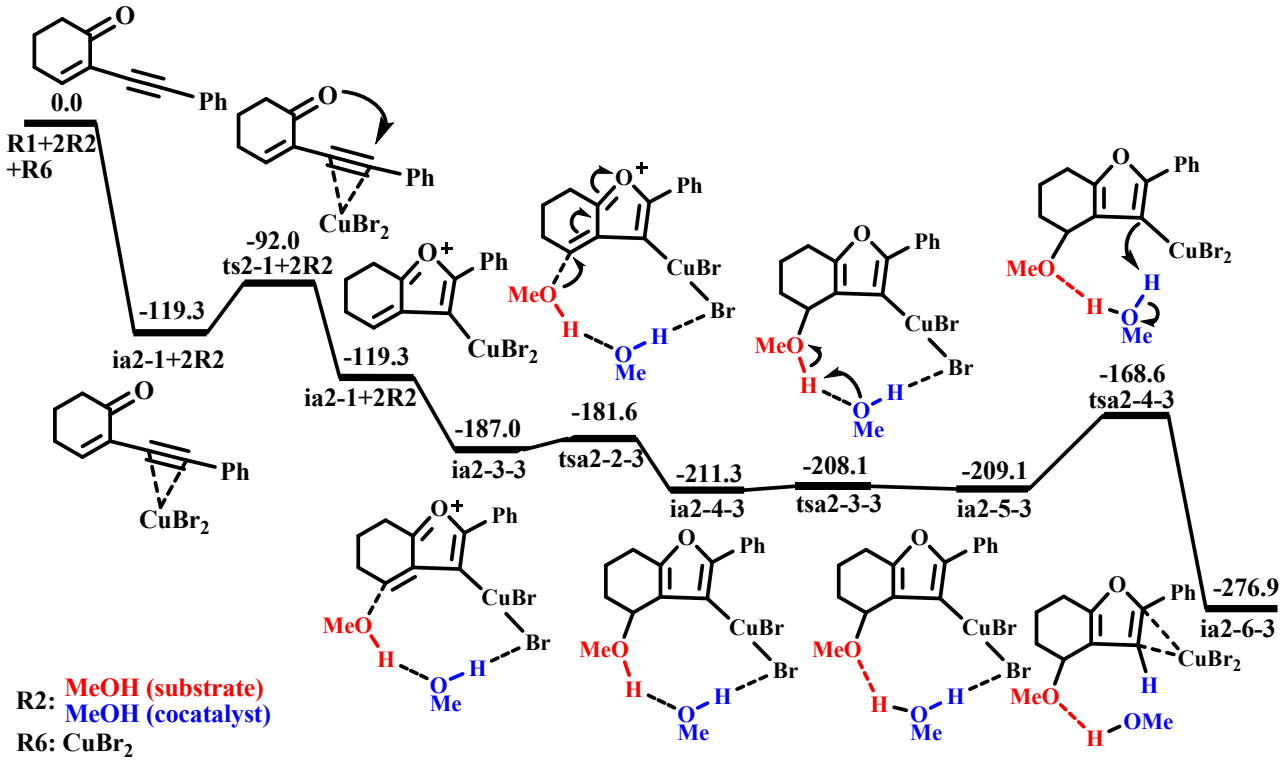

Figure S12. Optimal energy profile for the $CuBr_2$-catalyzed synthesis of highly substituted furans with the participation of MeOH.

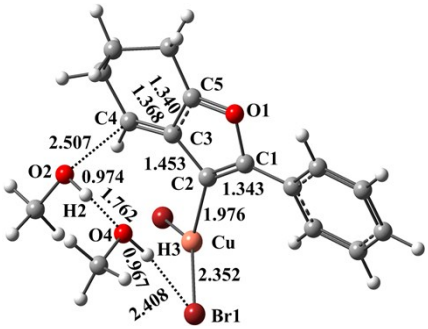

ia2-3-3

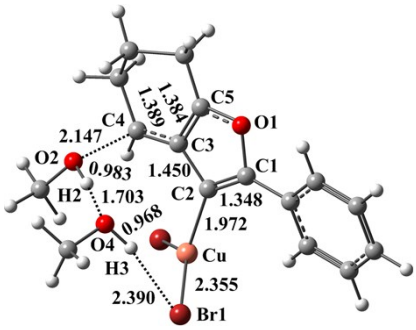

tsa2-2-3

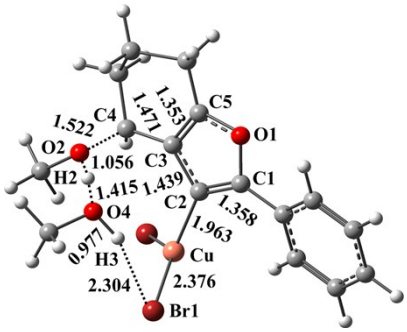

ia2-4-3

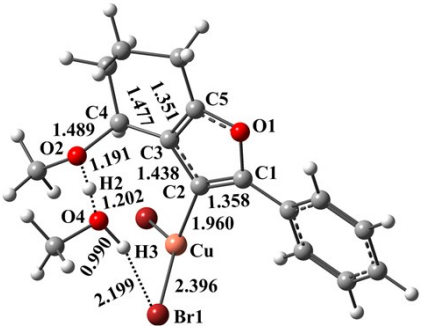

tsa2-3-3

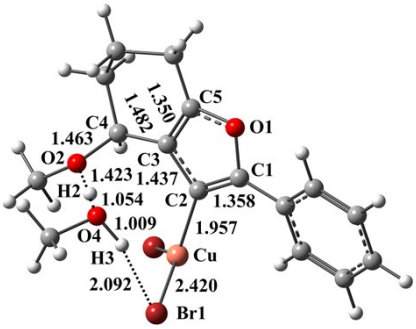

ia2-5-3

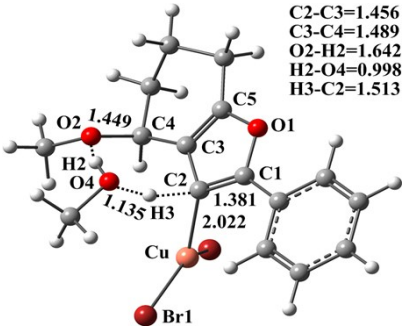

tsa2-4-3

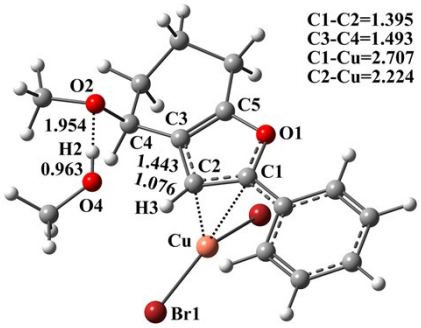

ia2-6-3

Figure S13. Optimized structures for the $CuBr_2$-catalyzed synthesis of high substituted furans with the participation of MeOH (selected structural parameters are listed (bond lengths in Å)).

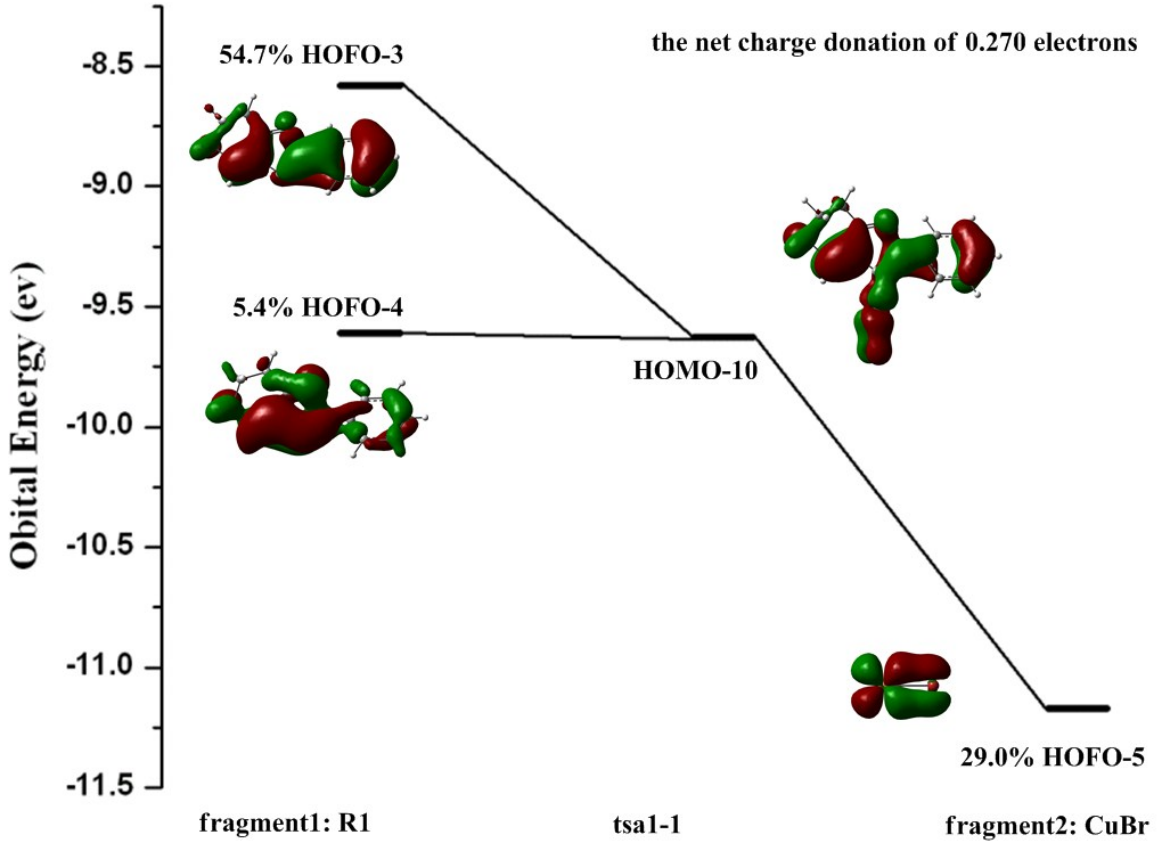

Figure S14. The orbital interaction diagram illustrating the coupling of the R1 and CuBr fragments in the tsa1-1 complex (the AOMix-CDA calculation at the BHandHLYP/6-31G* level; the net charge donation, is 0.270 electrons from fragment 1 to fragment 2).

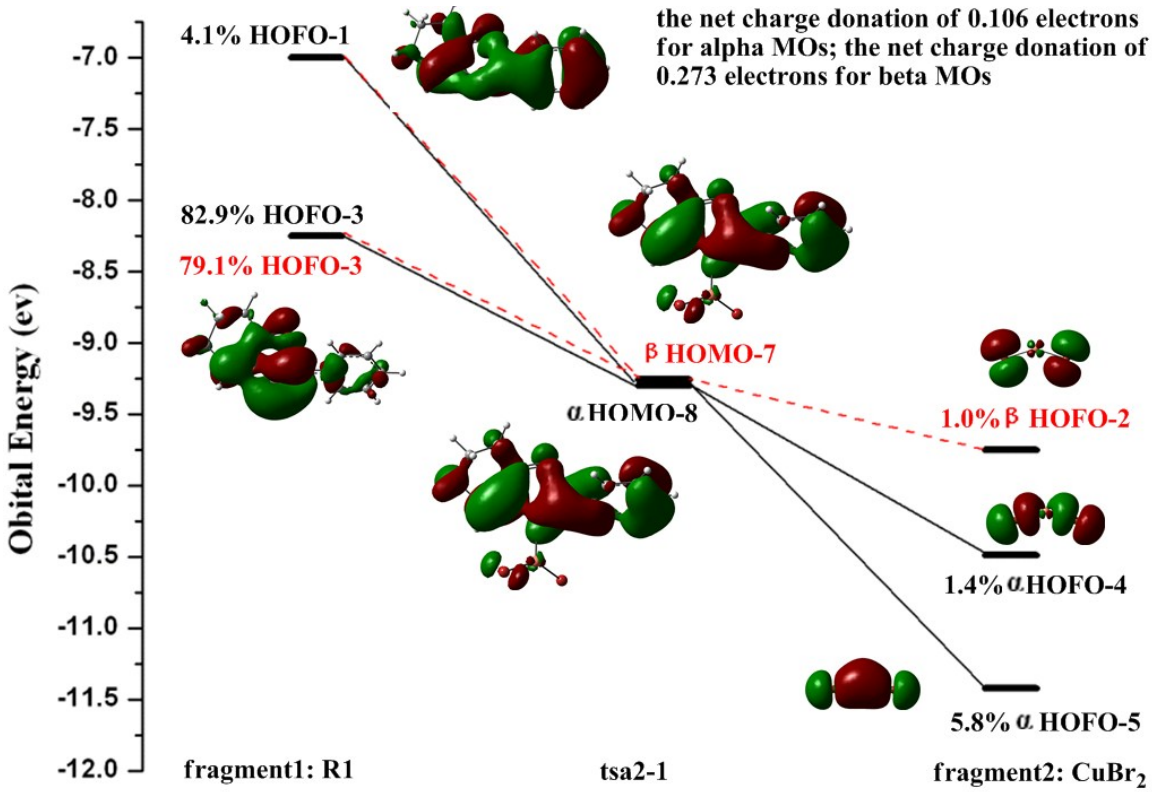

Figure S15. α, β-Spin orbital interaction diagram illustrating the coupling of the R1 and $CuBr_2$ fragments in the tsa2-1 complex (the AOMix-CDA calculation at the BHandHLYP/6-31G* level; α, β-MOs are shown in black and red respectively; the net charge donation, including the net charge donation of 0.106 electrons for alpha MOs and the charge donation of 0.273 electrons for beta MOs, is 0.379 electrons from fragment 1 to fragment 2).

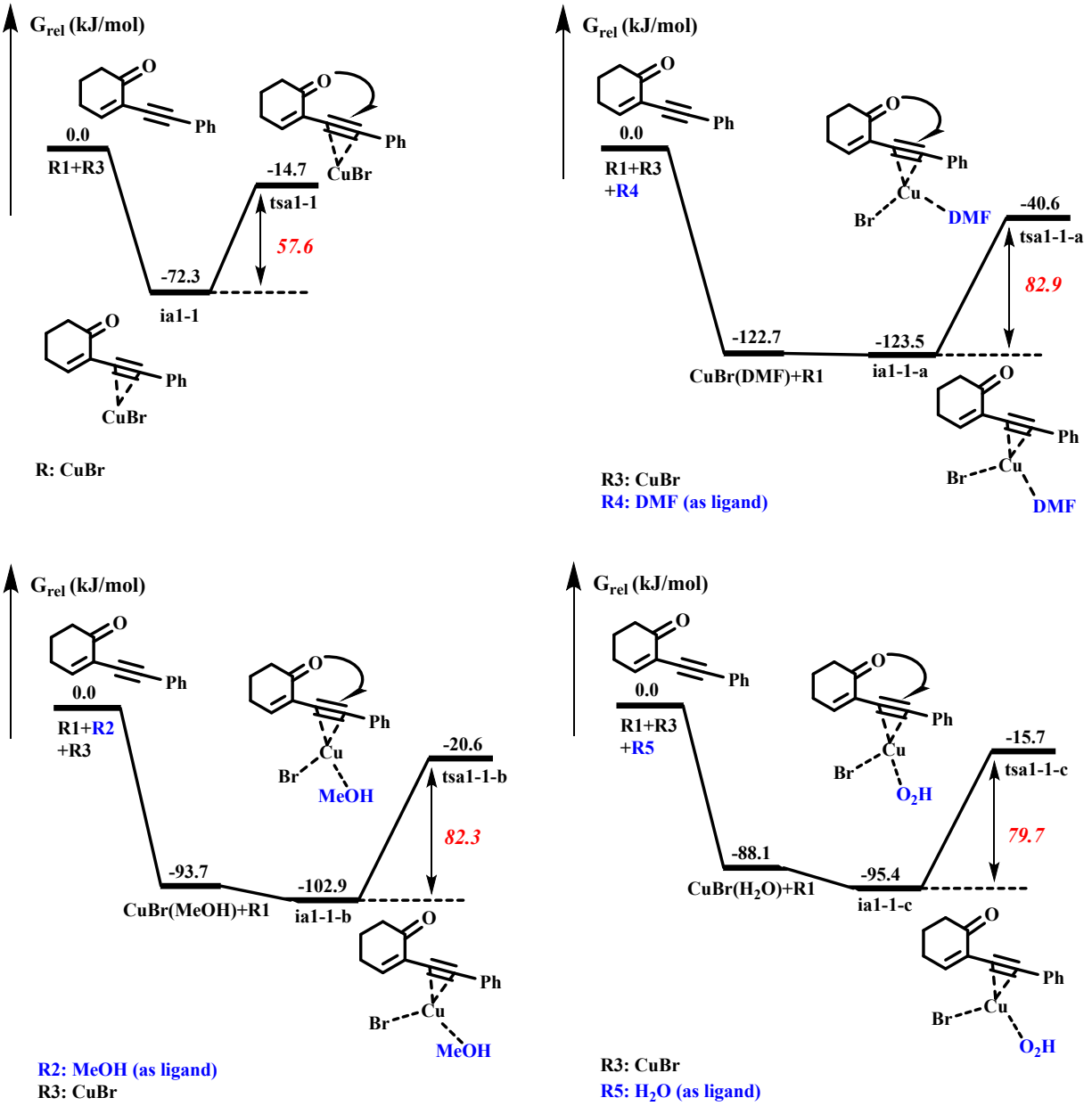

Figure S16. Comparison of the energy barriers for intramolecular cyclization reaction without and with DMF, MeOH or H_2O as a ligand.

CuBr coordinates with DMF, MeOH and H_2O to form new catalytic species CuBr(DMF), CuBr(MeOH) and CuBr(H_2O). However, our conclusions show that coordination of CuBr with DMF, MeOH or H_2O do not alter the reaction mechanism of intramolecular cyclization process, and the energy barrier of CuBr(DMF)-, CuBr(MeOH)- and CuBr(H_2O)-catalyzed cyclization reaction are 82.9, 82.3 and 79.7 kJ/mol, respectively, which are 25.3, 24.7 and 22.1 kJ/mol higher than that of the case without DMF, MeOH or H_2O as the ligand. Therefore, the effect of DMF, MeOH or H_2O as the ligand is negative.

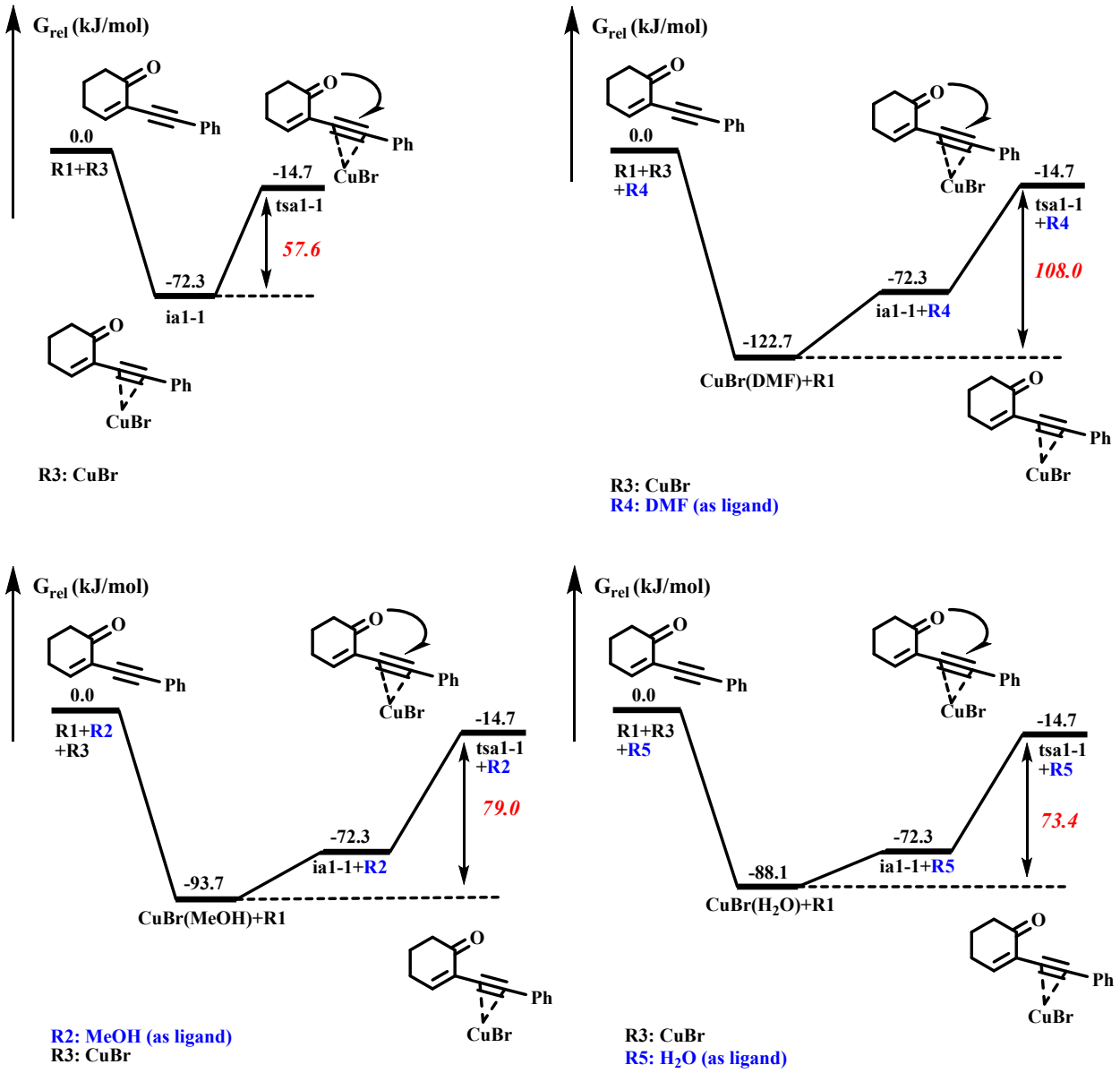

Figure S17. The effect of ligand exchanges (from DMF to R1, from MeOH to R1 and H_2O to R1) on the energy barriers of intramolecular cyclization process.

The new catalytic species CuBr(DMF), CuBr(MeOH) and CuBr(H_2O) are firstly formed by the coordination of CuBr with DMF, MeOH and H_2O, and then the ligands DMF, MeOH and H_2O of CuBr(DMF), CuBr(MeOH) and CuBr(H_2O) are exchanged by the triple bond of the substrate R1 to get intermediate ia1-1. However, the ligand exchanges (from DMF to R1, from MeOH to R1 and H_2O to R1) also do not alter the reaction mechanism of intramolecular cyclization process. In these cases, the energy barriers of cyclization reaction are 108.0, 79.0 and 73.4 kJ/mol, respectively, which are 50.4, 21.4 and 15.5 kJ/mol higher than that of the case without DMF, MeOH or H_2O as the ligand. Obviously, the ligand exchanges of DMF, MeOH and H_2O with triple bond of the substrate R1are negative for the cyclization reaction.

Table S1. The test of BHandHLYP, B3LYP and BLYP by comparing the rate-limiting energy barriers from ima1-1 to tsa1-3-1.

Methods	Species	Free Energies (a.u)	Rate-Limiting Energy Barriers (kJ/mol)
BHandHLYP	ia1-1+R2	-3501.5171996	
BHandHLYP	tsa1-3-1	-3501.4806262	96.0
B3LYP	ia1-1+R2	-3502.2181417	
B3LYP	tsa1-3-1	-3502.1826451	93.2
BLYP	ia1-1+R2	-3501.8757734	
BLYP	tsa1-3-1	-3501.8357860	105.0

The limiting-rate energy barriers from ia1-1 to tsa1-3-1 (see Figure 1) are 96.0 (BHandHLYP), 93.2 (B3LYP) and 105.0 (BLYP) kJ/mol in the CuBr-catalyzed synthesis of highly substituted furans without the participation of cocatalyst, respectively. The difference values of 2.8 (96.0 vs 93.2) and 9.0 (96.0 vs 105.0) kJ/mol are very small, which do not affect the calculational results. Therefore, using BHandHLYP method to study our present system is reliable.

Table S2. To explore effect of basis sets 6-31g*,6-31+g*, 6-31g** and 6-311g* by comparing the rate-limiting energy barriers from ia1-1 to tsa1-3-1.

Basis Sets	Species	Free Energies (a.u)	Rate-Limiting Energy Barriers (kJ/mol)
6-31g*	ia1-1+R2	-3501.5171996	
6-31g*	tsa1-3-1	-3501.4806262	96.0
6-31+g*	ia1-1+R2	-3501.5175492	
6-31+g*	tsa1-3-1	-3501.4809735	96.0
6-31g**	ia1-1+R2	-3501.5172291	
6-31g**	tsa1-3-1	-3501.4804738	96.5
6-311g*	ia1-1+R2	-3501.5177538	
6-311g*	tsa1-3-1	-3501.4810921	96.3

The rate-limiting energy barriers from ia1-1 to tsa1-3-1 (see Figure 1) are 96.0 (6-31g*), 96.0 (6-31+g*), 96.5 (6-31g**) and 96.3 (6-311g*) kJ/mol in the CuBr-catalyzed synthesis of highly substituted furans without the participation of cocatalyst, respectively. Obviously, the application of large basis sets 6-31+g*, 6-31g** and 6-311g* do not give a better result than that of 6-31g*. In order to save computational cost, 6-31g* is selected as the economical basis set used in our present system.

Intrinsic reaction coordinate (IRC)

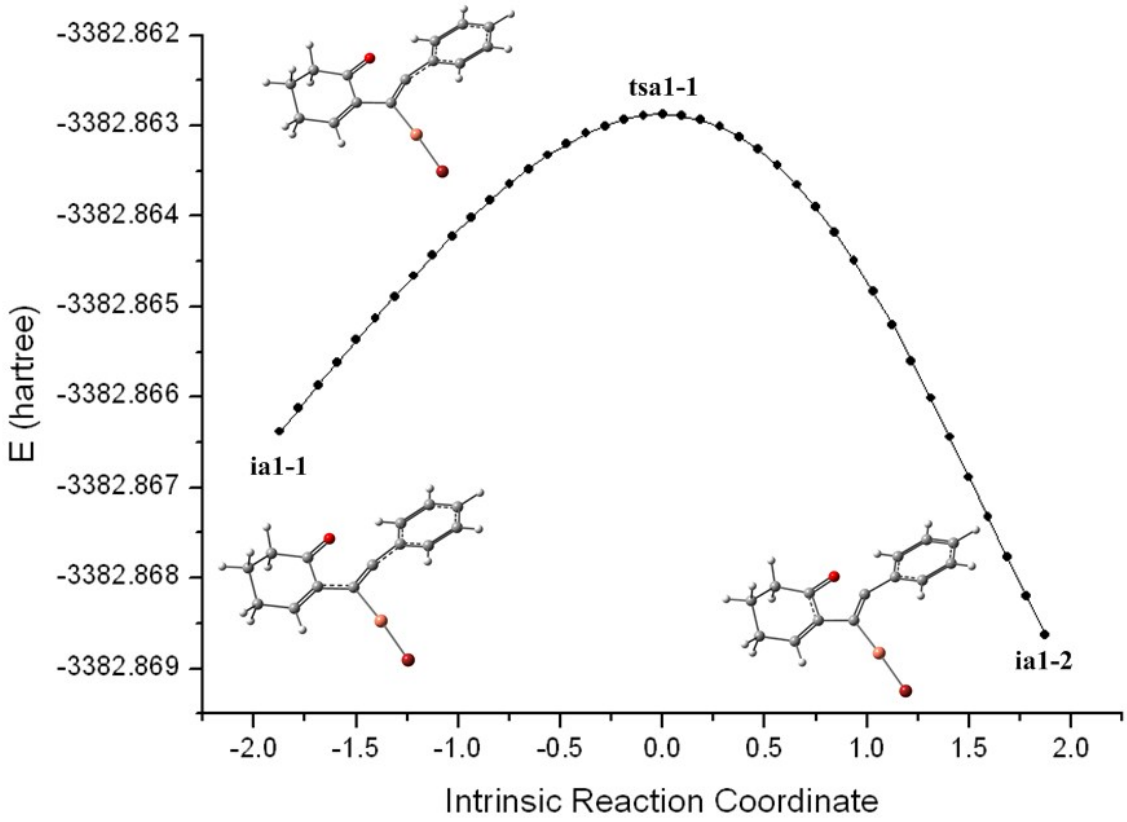

Figure S18. Intrinsic reaction coordinate (IRC) of tsa1-1.

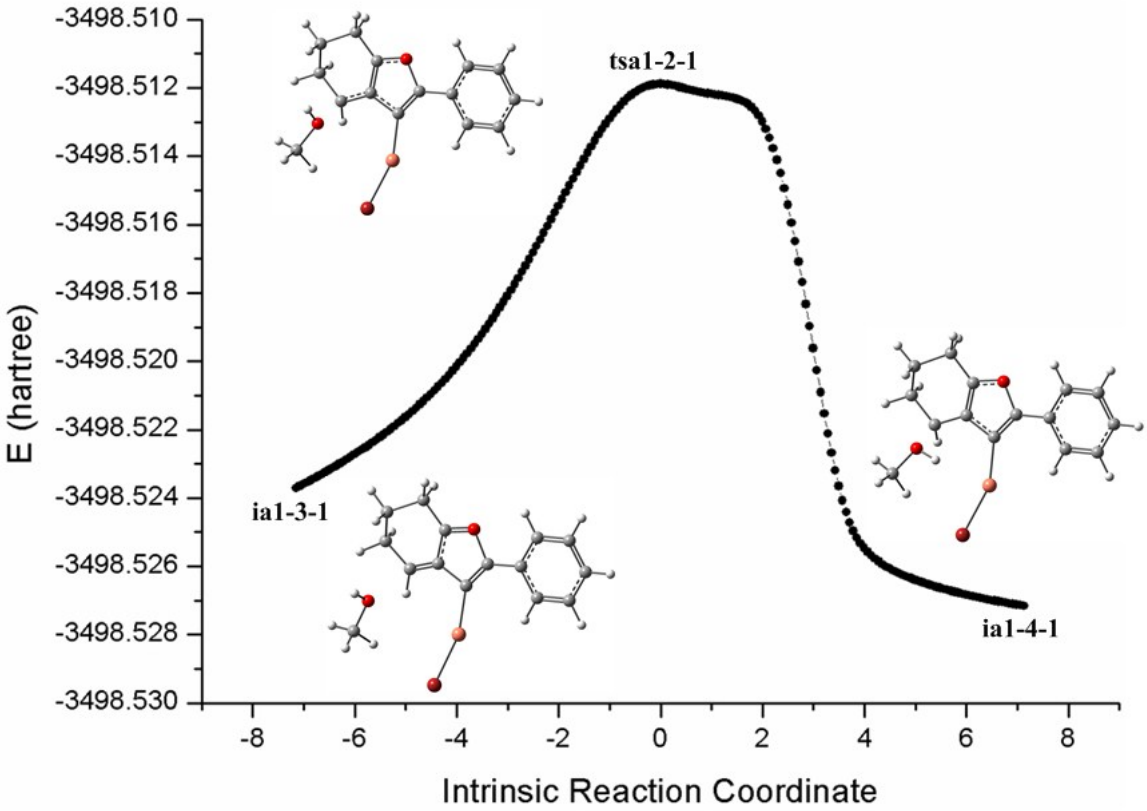

Figure S19. Intrinsic reaction coordinate (IRC) of tsa1-2-1.

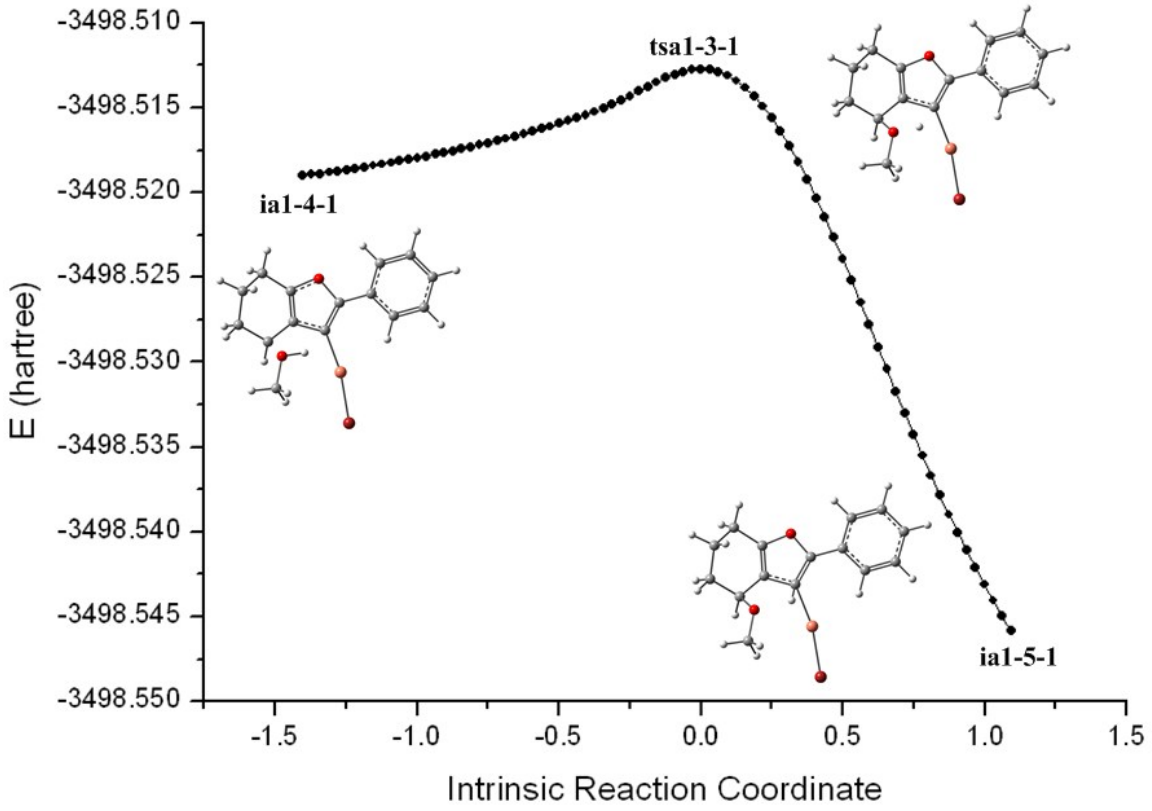

Figure S20. Intrinsic reaction coordinate (IRC) of tsa1-3-1.

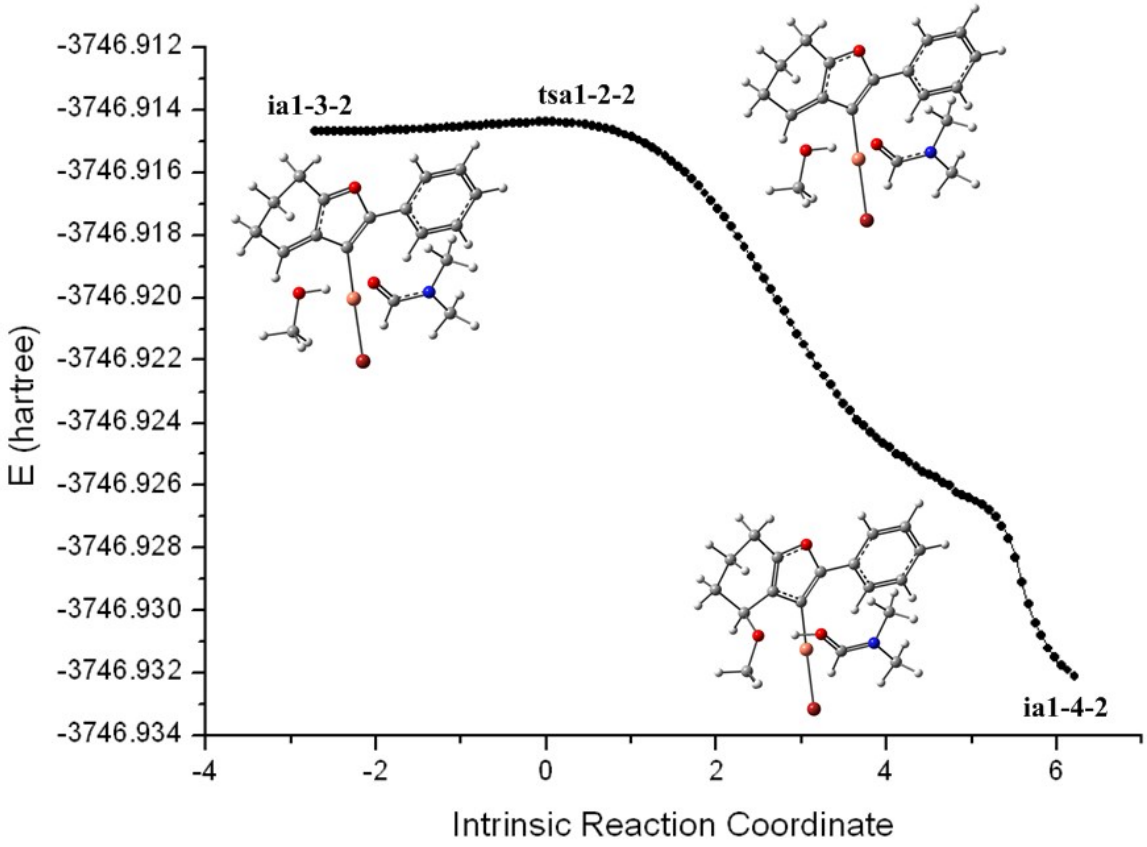

Figure S21. Intrinsic reaction coordinate (IRC) of tsa1-2-2.

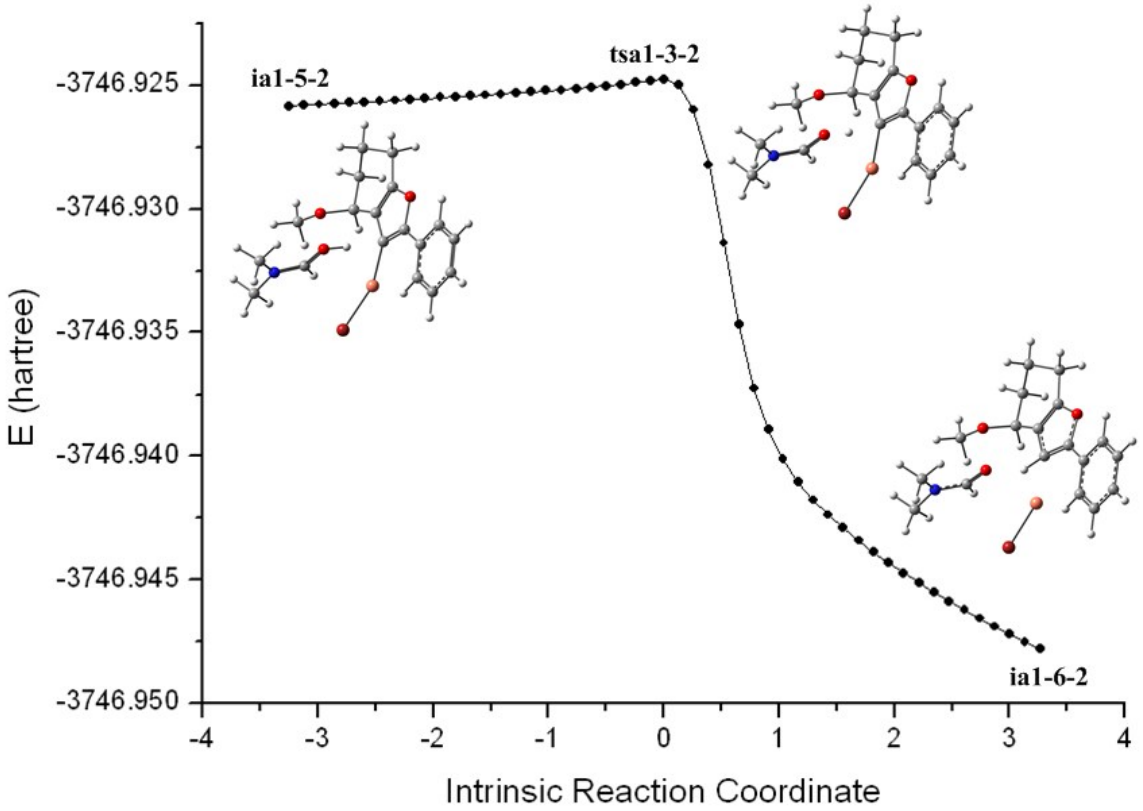

Figure S22. Intrinsic reaction coordinate (IRC) of tsa1-3-2.

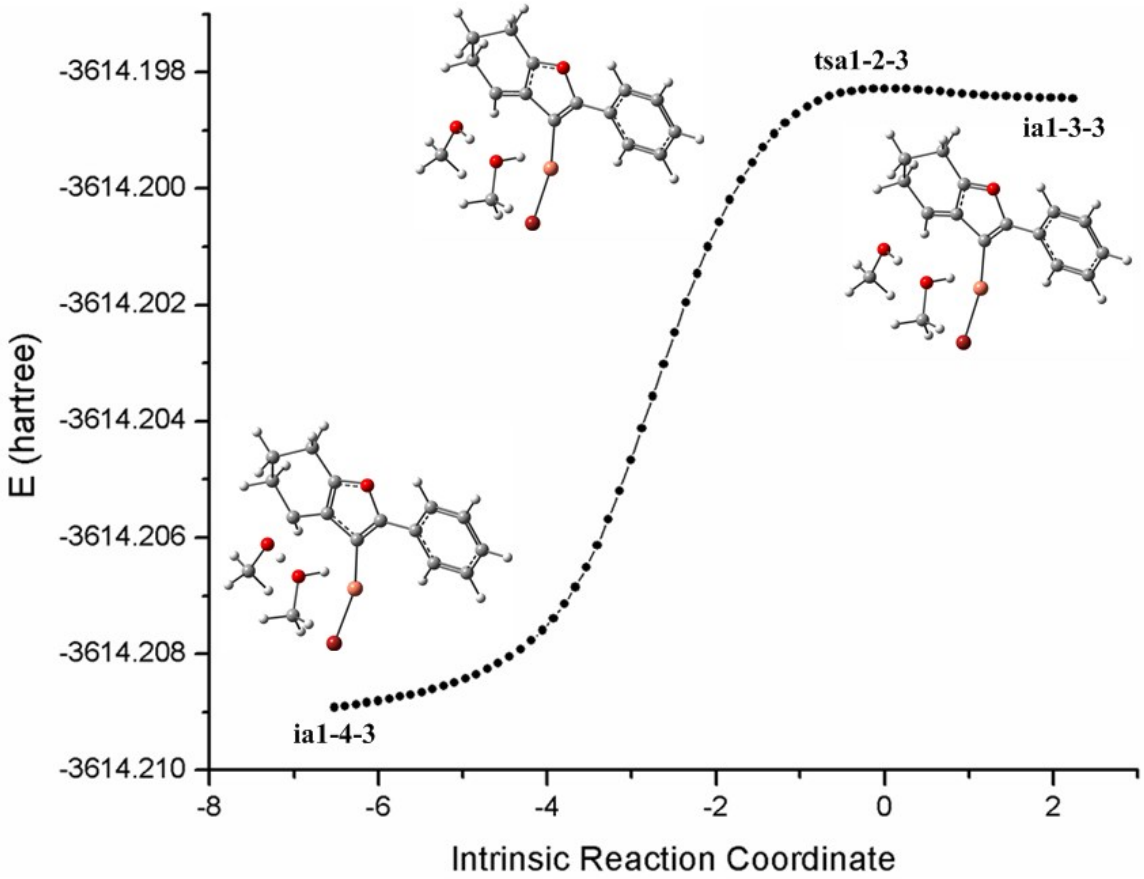

Figure S23. Intrinsic reaction coordinate (IRC) of tsa1-2-3.

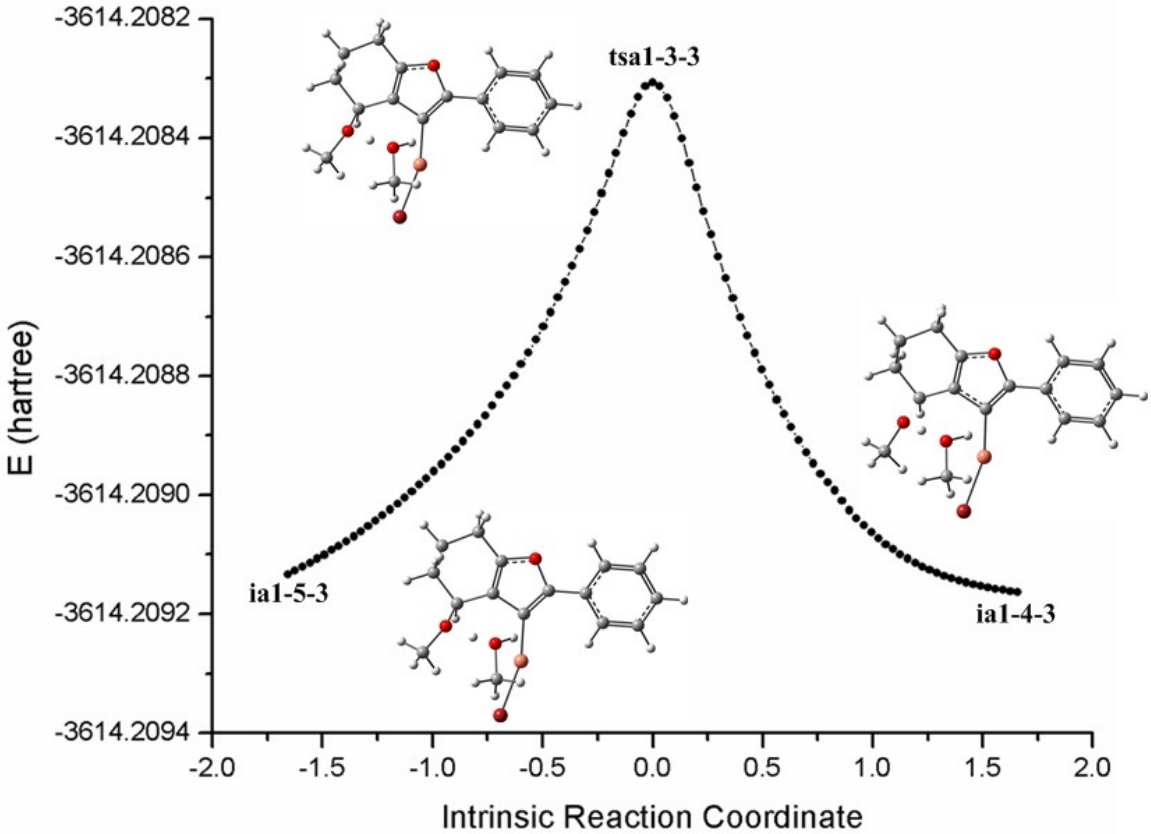

Figure S24. Intrinsic reaction coordinate (IRC) of tsa1-3-3.

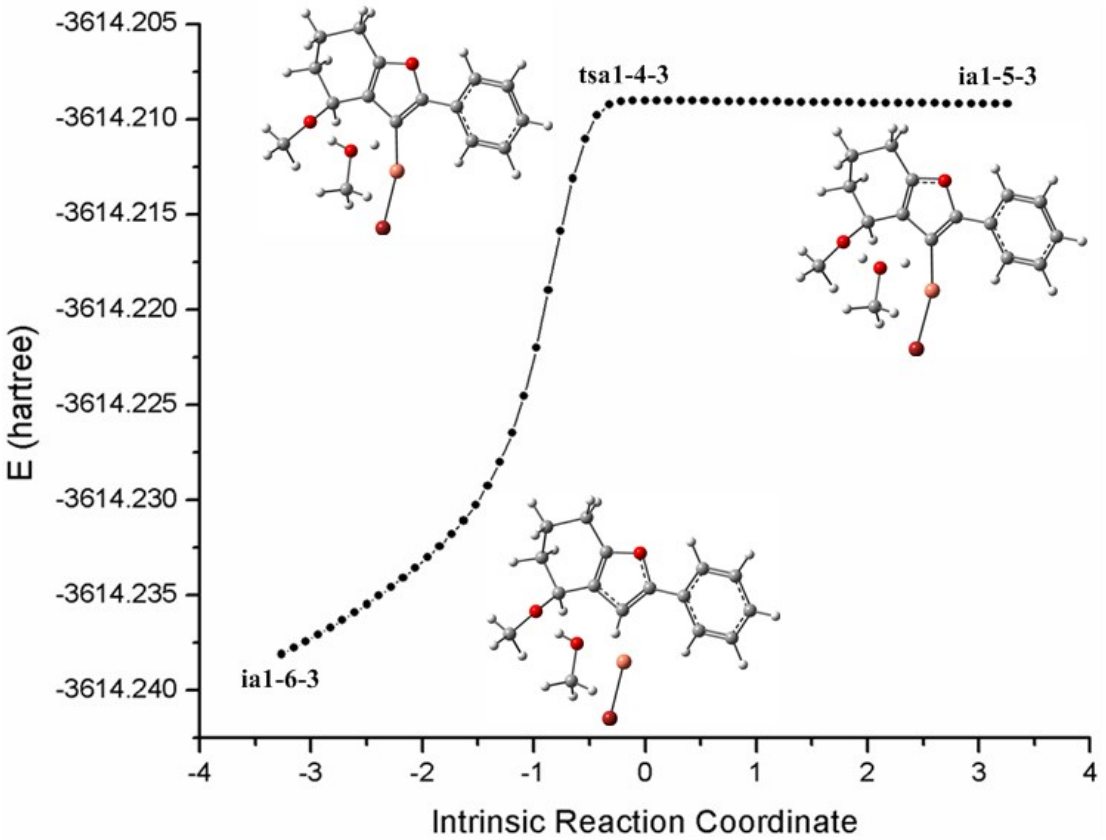

Figure S25. Intrinsic reaction coordinate (IRC) of tsa1-4-3.

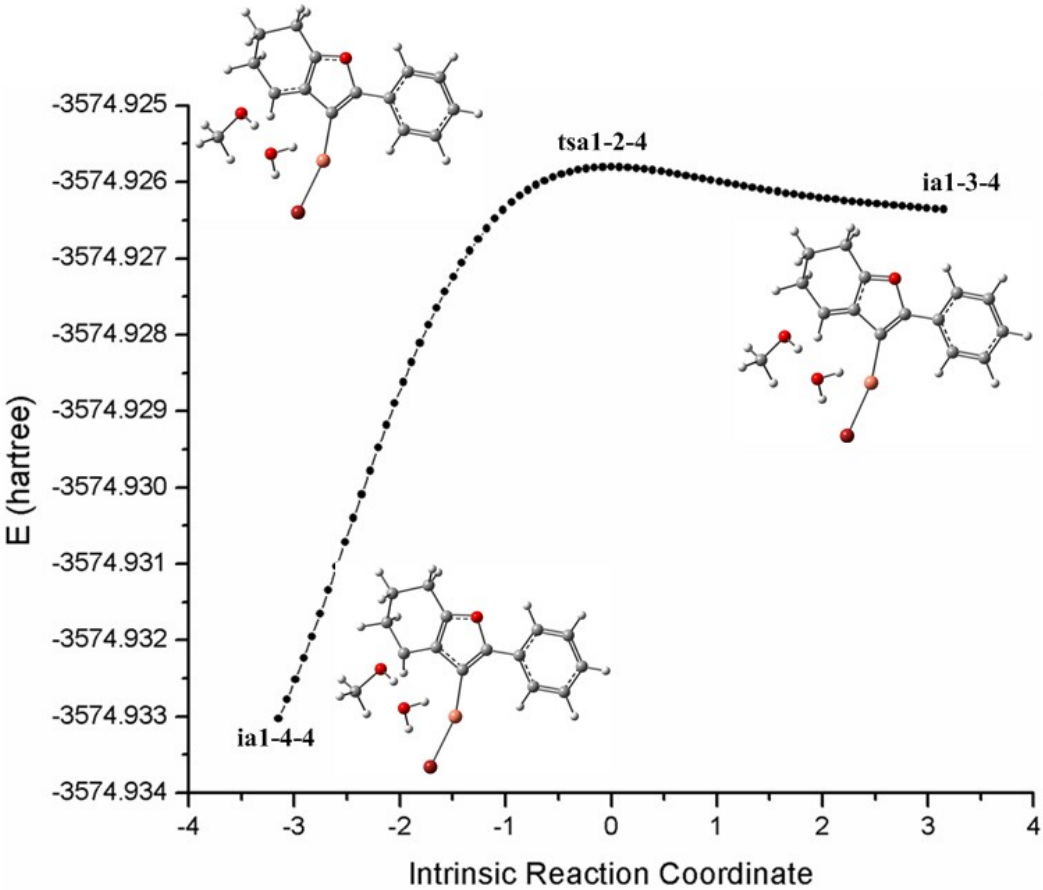

Figure S26. Intrinsic reaction coordinate (IRC) of tsa1-2-4.

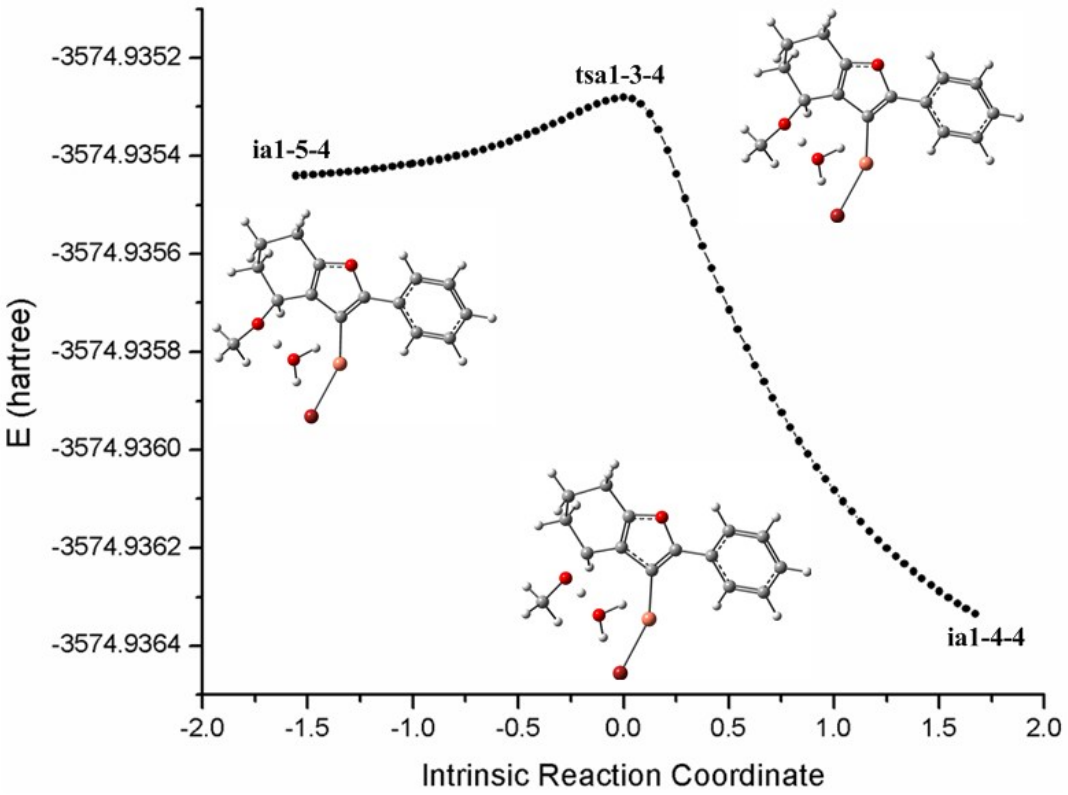

Figure S27. Intrinsic reaction coordinate (IRC) of tsa1-3-4.

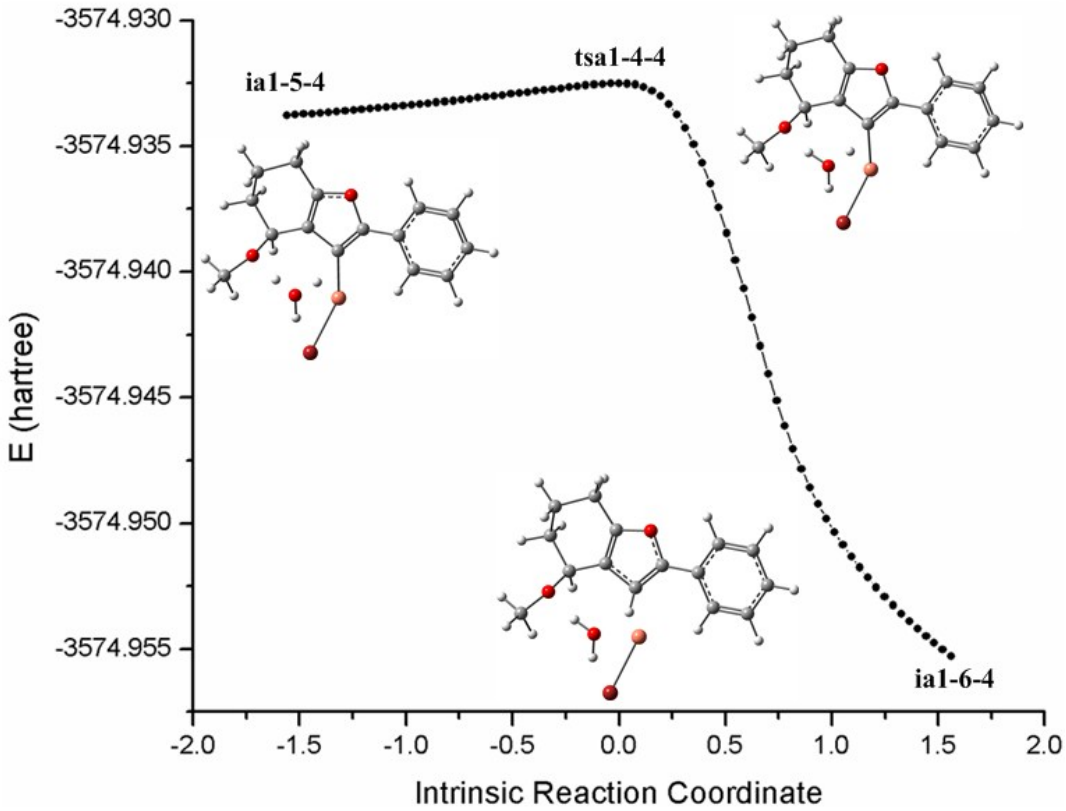

Figure S28. Intrinsic reaction coordinate (IRC) of tsa1-4-4.

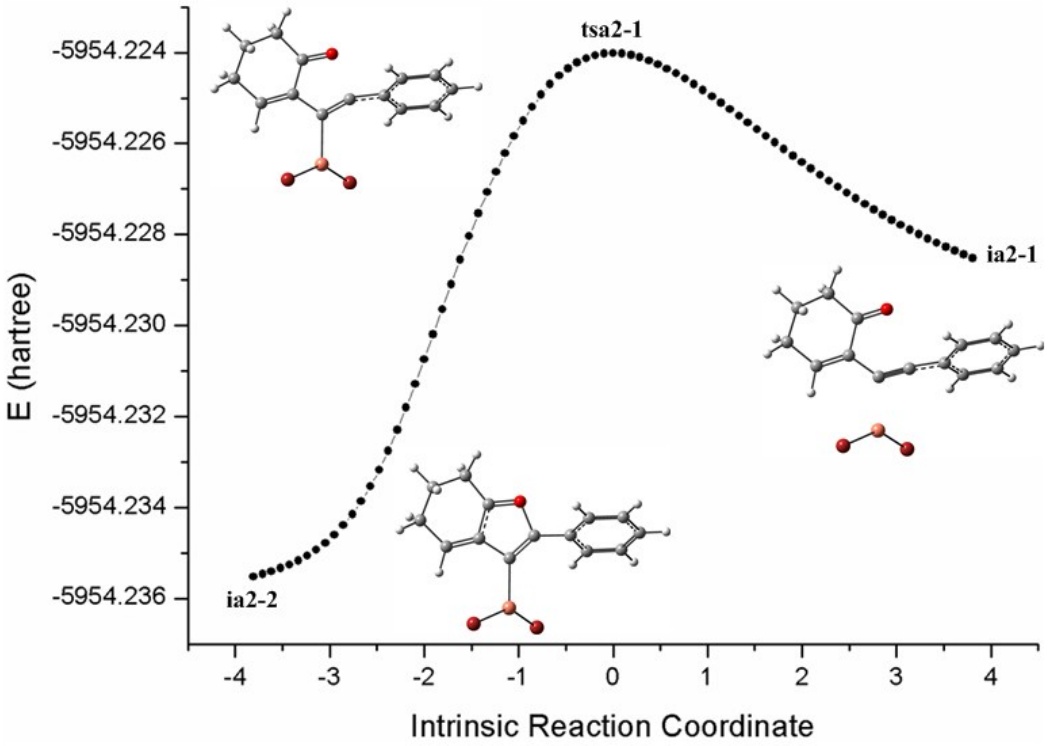

Figure S29. Intrinsic reaction coordinate (IRC) of tsa2-1.

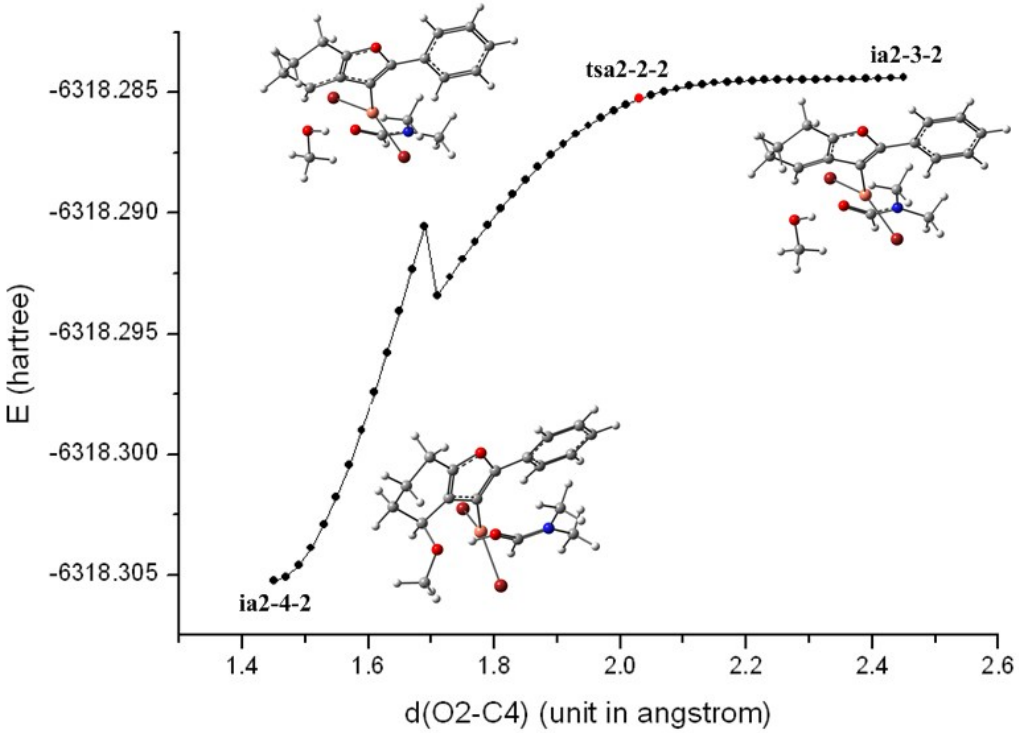

Figure S30. loose scan profile from ia2-4-2 to ia2-3-2 along breakage of the O2-C4 bond (from 1.450 to 2.450 Å).

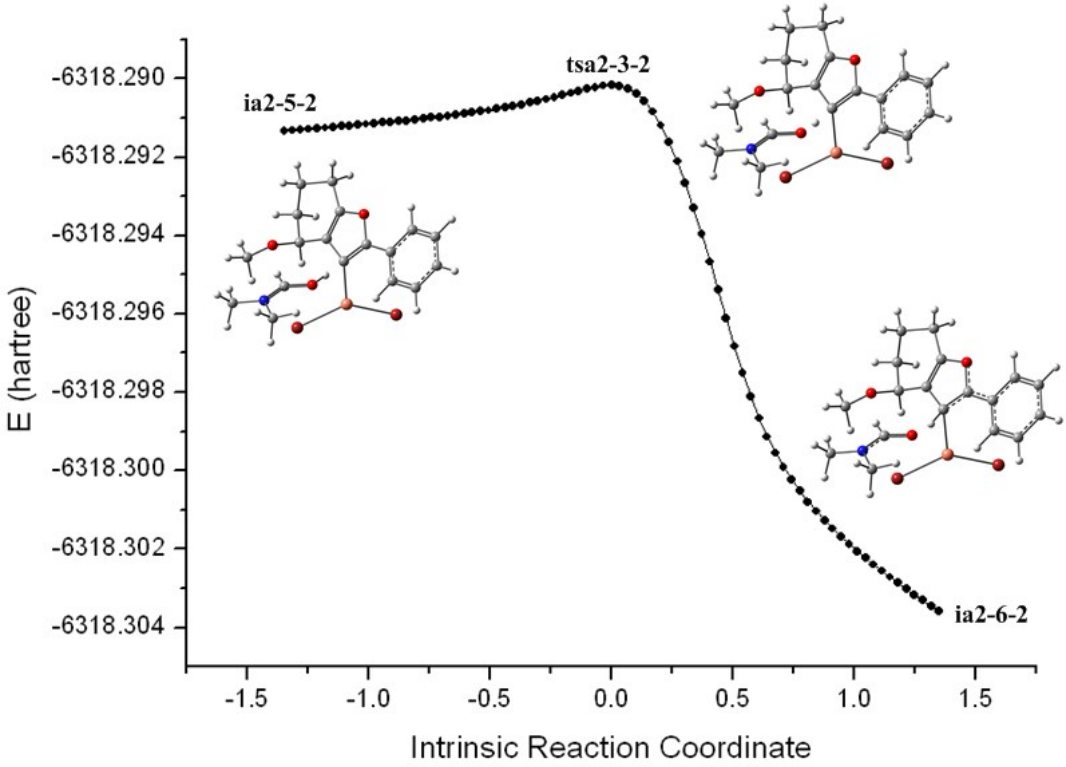

Figure S31. Intrinsic reaction coordinate (IRC) of tsa2-3-2.

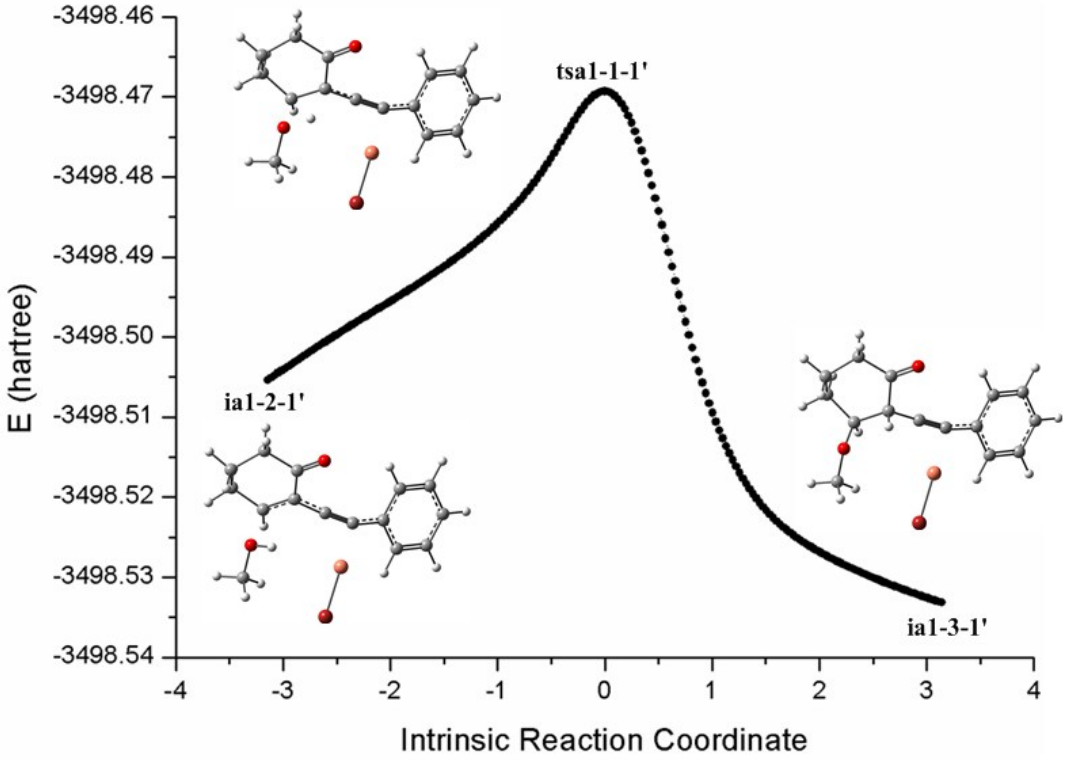

Figure S32. Intrinsic reaction coordinate (IRC) of tsa1-1-1'.

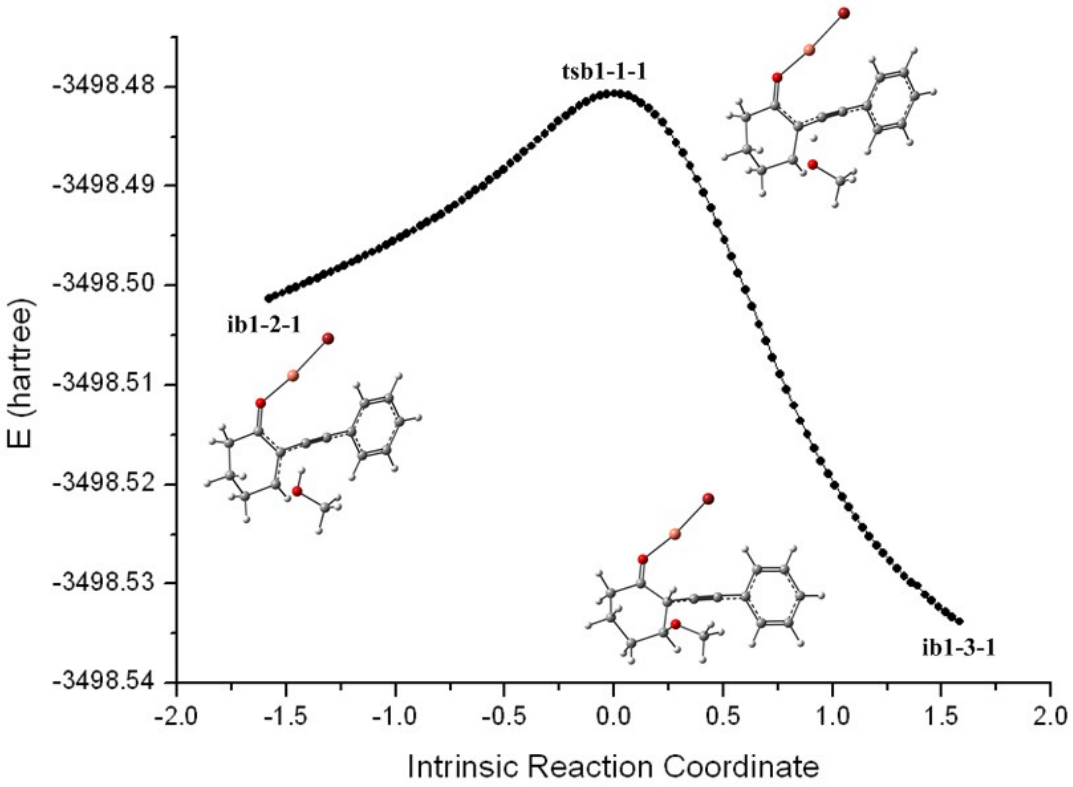

Figure S33. Intrinsic reaction coordinate (IRC) of tsb1-1-1.

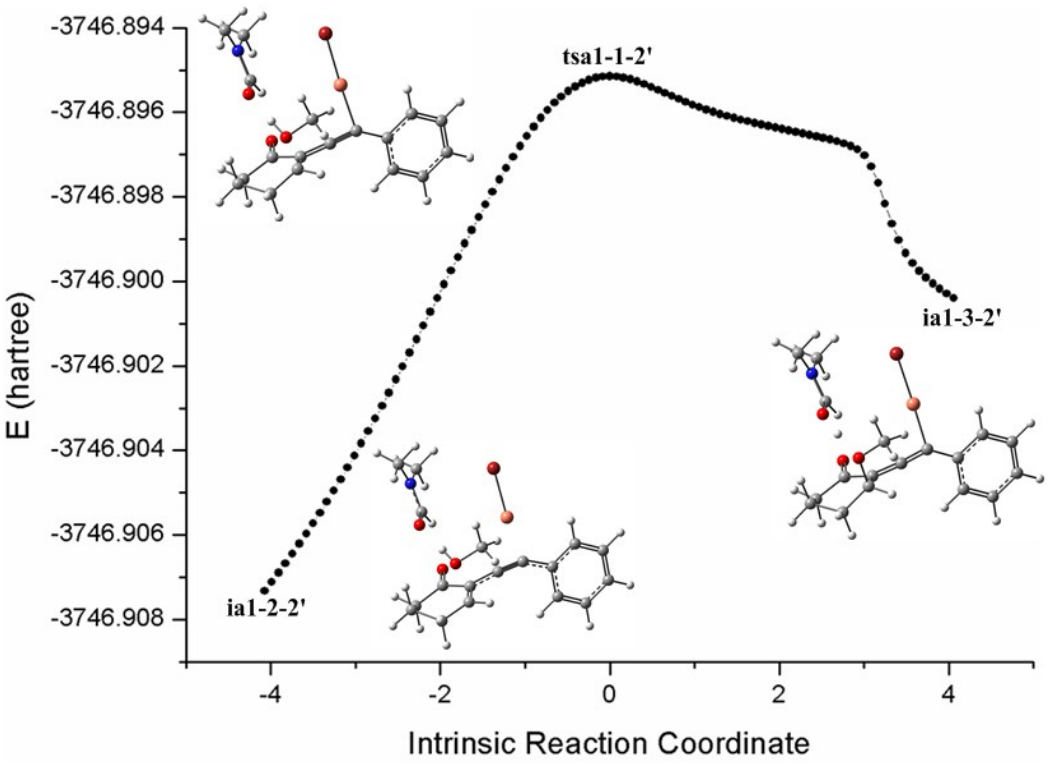

Figure S34. Intrinsic reaction coordinate (IRC) of tsa1-1-2'.

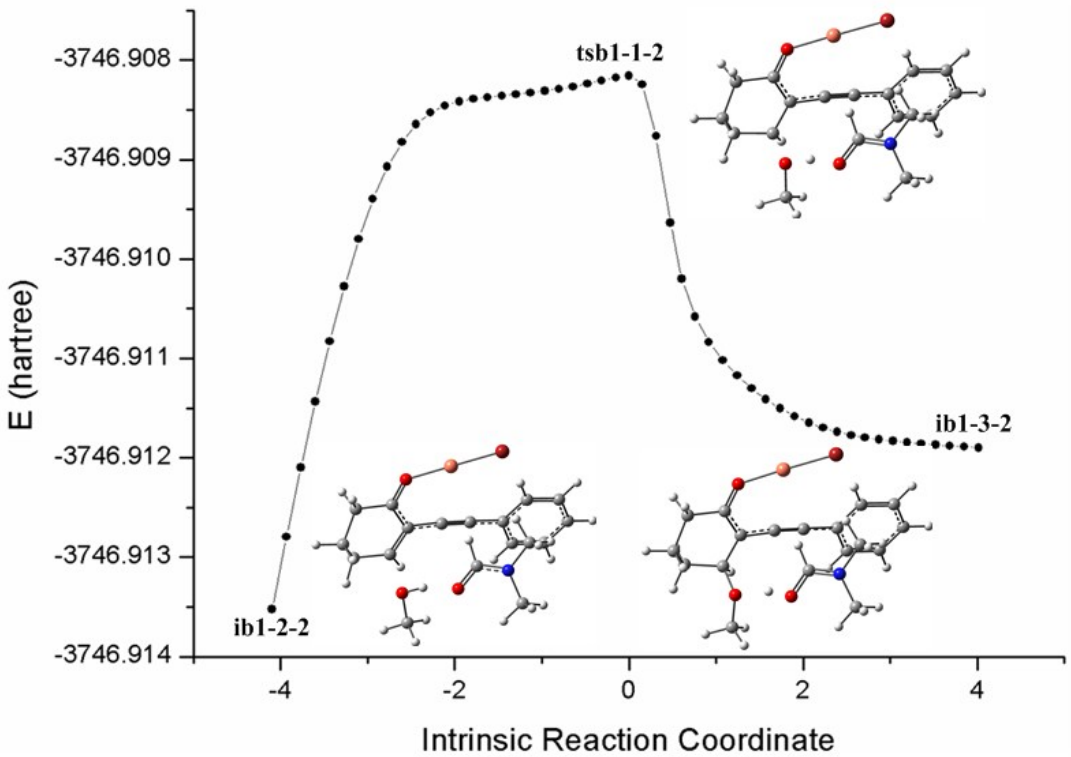

Figure S35. Intrinsic reaction coordinate (IRC) of tsb1-1-2.

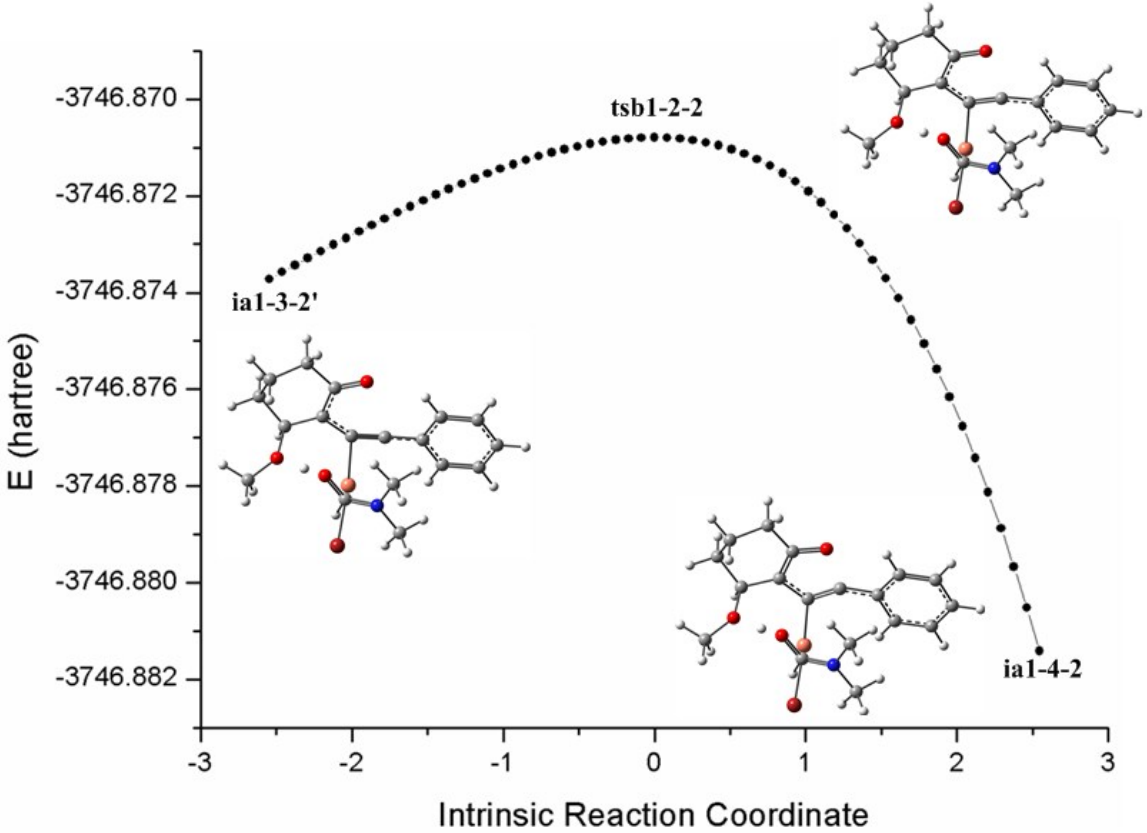

Figure S36. Intrinsic reaction coordinate (IRC) of tsb1-2-2.

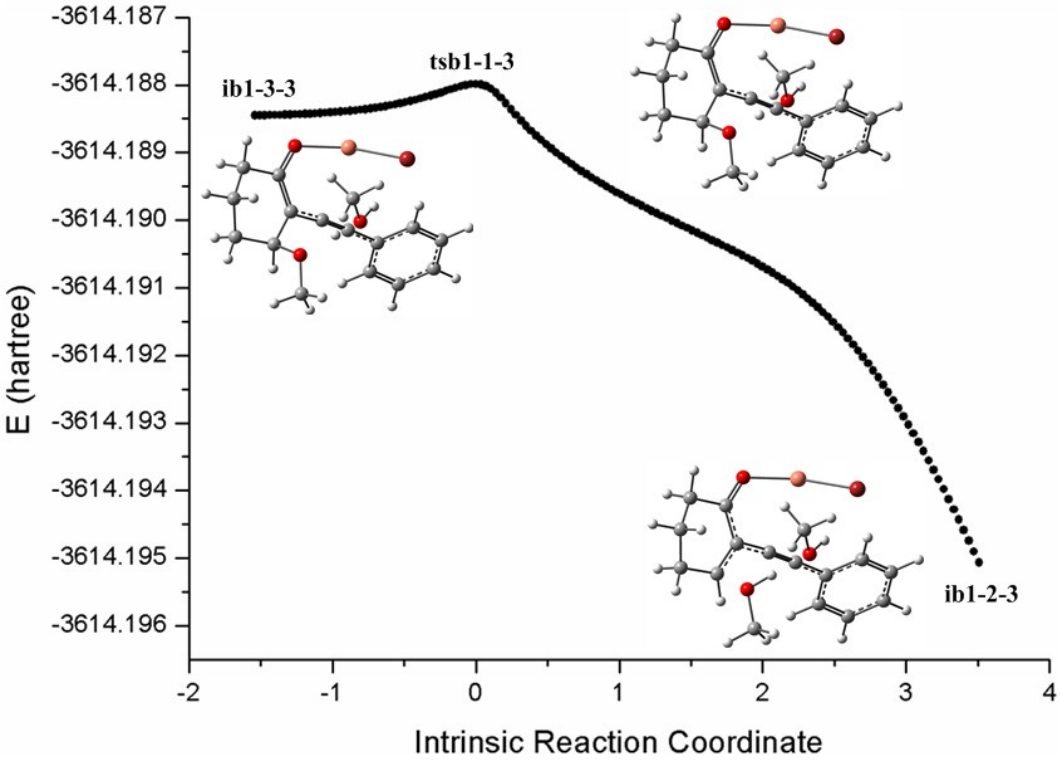

Figure S37. Intrinsic reaction coordinate (IRC) of tsb1-1-3.

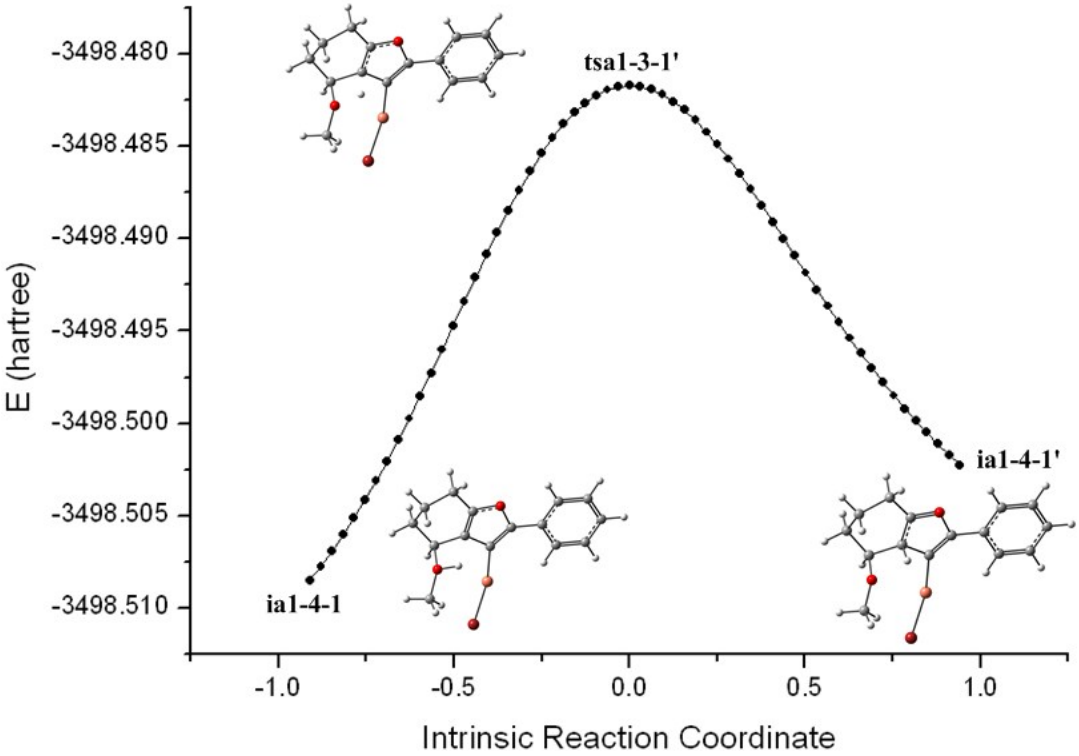

Figure S38. Intrinsic reaction coordinate (IRC) of tsa1-3-1'.

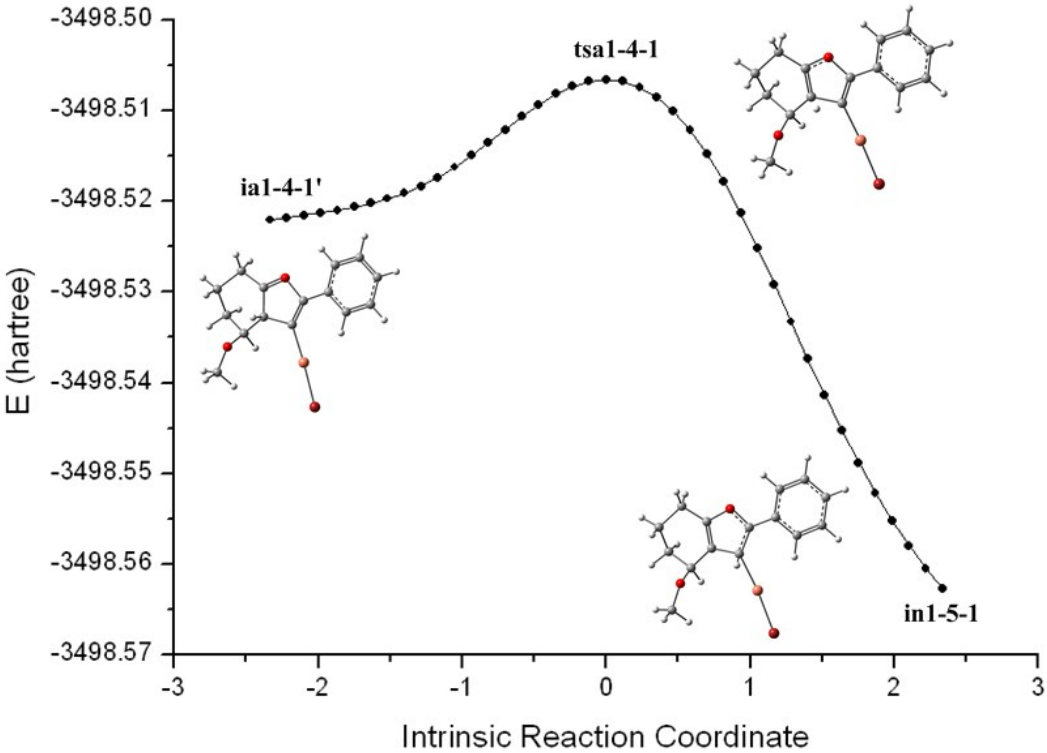

Figure S39. Intrinsic reaction coordinate (IRC) of tsa1-4-1.